PAPER

Hybrid *α*-attractors, primordial black holes and gravitational wave backgrounds

View the article online for updates and enhancements.

Hybrid α-attractors, primordial black holes and gravitational wave backgrounds

Matteo Braglia,[a,b] **Andrei Linde,**[c] **Renata Kallosh**[c] **and Fabio Finelli**[b,d]

[a]Center for Cosmology and Particle Physics, New York University,
  726 Broadway, New York, NY 10003, U.S.A.

[b]INAF/OAS Bologna,
  via Gobetti 101, I-40129 Bologna, Italy

[c]Stanford Institute for Theoretical Physics and Department of Physics,
  Stanford University, Stanford, CA 94305, U.S.A.

[d]INFN, Sezione di Bologna,
  via Irnerio 46, I-40126 Bologna, Italy

  E-mail: mb9289@nyu.edu, alinde@stanford.edu, kallosh@stanford.edu,
  fabio.finelli@inaf.it

Abstract. We investigate the two-stage inflation regime in the theory of hybrid cosmological α-attractors. The spectrum of inflationary perturbations is compatible with the latest Planck/BICEP/Keck Array results, thanks to the attractor properties of the model. However, at smaller scales, it may have a very high peak of controllable width and position, leading to a copious production of primordial black holes (PBH) and generation of a stochastic background of gravitational waves (SGWB).

Contents

1 Introduction

There has recently been a growing interest in the possibility to generate large peaks in the amplitude of perturbations at the late stages of inflation. Such peaks may lead to the formation of primordial black holes (PBHs) and to generate a stochastic gravitational wave background (SGWB) which can be explored with future gravitational wave interferometers.

One of the first fully developed models to generate such peaks in the primordial power spectrum (PPS) of the perturbations and consequently seed PBH formation was proposed in [1] in the context of the hybrid inflation scenario [2, 3]. There, it was argued that under certain conditions such PBHs may provide a significant contribution to dark matter. Many other interesting mechanisms were proposed to produce a bump in the PPS from inflation. Among them is the PBH production due to large isocurvature perturbations [4], amplification of perturbations during rapid turns of inflationary trajectory [5–11], a sudden slowing down of the inflaton evolution often referred to as Ultra Slow Roll [12–22] or other types of features [23–29] and creation of black holes and wormholes by colliding walls [30, 31]. For a review of these and other mechanisms of PBH formation and their cosmological implications see e.g. [32–34].

In this paper, we will revisit the mechanism of [1] in the recently proposed α-attractor generalization [35] (see also [36]) of the hybrid inflation scenario [2, 3] and consider its consequences on PBH and SGWB production. While, due to the large uncertainties in the critical process of PBH formation, we will just touch upon it, we will instead provide a full characterization of the SGWB produced by the large perturbations at horizon re-entry during the radiation dominated era [37–39] (see e.g. [40] for a review), which can be used in the future to test this model. We will pay particular attention to the consistency with large scale measurements of the Cosmic microwave Background (CMB) anisotropies from the latest Planck/BICEP/Keck Array release [41–43], which is not a trivial task since models producing

a peak in the small scale power spectrum often tend to predict a spectral index which is slightly redder than the Planck best fit.

Let us start with a quick reminder of the basic hybrid inflation model [2, 3]. The effective potential of this model is given by

$$V(\chi, \phi) = \frac{1}{4\lambda}(M^2 - \lambda\chi^2)^2 + \frac{m^2}{2}\phi^2 + \frac{g^2}{2}\phi^2\chi^2. \tag{1.1}$$

For $\phi > \phi_c = M/g$ the only minimum of the effective potential $V(\chi, \phi)$ with respect to χ, sometimes referred to as *hybrid field*, is at $\chi = 0$. The mass squared of the field χ at $\chi = 0$ is equal to $V_{\chi,\chi}(\chi = 0) = -M^2 + g^2\phi^2$. At large ϕ, the curvature of the effective potential in the χ-direction is much larger than in the ϕ-direction. Thus, during the first stages of expansion of the universe, the field χ rolls down to $\chi = 0$, whereas the field ϕ could remain large and drive inflation for a much longer time. At that time, the potential of the inflaton field ϕ is given by $V(\phi) = \frac{m^2}{2}\phi^2 + V_{\text{uplift}}$, where the uplift potential is given by $\frac{M^2}{4\lambda}$.

At the moment when the inflaton field ϕ becomes smaller than $\phi_c = M/g$, the effective mass squared of the field χ at $\chi = 0$ becomes negative (tachyonic), quantum fluctuations of this field begin to grow, and a so-called *waterfall* phase transition with symmetry breaking occurs.

In the simplest versions of the hybrid inflation scenario, the absolute value of the tachyonic mass of the field χ becomes much greater than the Hubble constant H shortly after the field ϕ becomes smaller than ϕ_c. In that case, the tachyonic instability leads to an abrupt end of inflation at $\phi \approx \phi_c$ [2, 3]. However, in some models the tachyonic mass of the field χ at $\phi \lesssim \phi_c$ may remain much smaller than the Hubble constant H. In the Higgs-type potential $V(\chi) \sim (\chi^2 - \chi_0^2)^2$ used in [1–3], this regime occurs for $\chi_0 \gg 1$ (in Planck mass units $M_{\text{pl}} = 1$). In such cases, inflation continues while the field χ slowly rolls down towards the minimum of $V(\chi)$. As we will explain later, the amplitude of perturbations produced at the second stage of inflation in hybrid inflation models with such properties can be extremely large.

In fact, these perturbations can be so large that in addition to producing PBH they may also trigger the process of eternal inflation inside some regions of the observable part of the universe [1]. One way to avoid this problem and regularize the amplitude of the perturbations is to consider models with $\chi_0 \lesssim 1$ [1]. However, this does not solve the problem of superheavy topological defects in this scenario and in its various generalizations, such as the Clesse-Bellido model [44].

In this paper we are going to show that both of these problems can be solved by adding a tiny linear term $\sim \chi$ to the potential (1.1). As we will see, this allows to control the strength of the effect and the amplitude of the peak in the PPS, and simultaneously solve the problem of topological defects.

Whereas the basic mechanism of the PBH production described above [1] is quite general and can be implemented in a broad class of hybrid inflation models, the simplest versions of hybrid inflation [2, 3] resulted in the spectral index $n_s \approx 1 + 2m^2/V_{\text{uplift}} > 1$, which did not match the Planck data [45].

An attempt to overcome this problem was made in [44]. The authors changed the sign of m^2 making the inflaton potential tachyonic, $m^2 < 0$, which allowed to have $n_s < 1$. This paper, together with the detection of gravitational waves from a binary black hole merger by the LIGO-Virgo collaboration [46], attracted new attention to the possibility pointed out in [1] that PBH may constitute a substantial portion of the dark matter [47–49]. However, the tachyonic potential $V(\phi)$ used in the toy model discussed in [44] is unbounded from below, and the field $\phi \gtrsim \phi_c$ instead of moving towards $\phi = 0$ tends to run to $\phi \to \infty$. This makes

it difficult to solve the problem of initial conditions for inflation in this scenario unless the potential is further modified at $\phi > \phi_c$.

Fortunately, this problem can be addressed in the α-attractor versions [35] of the original hybrid inflation scenario [2, 3]. For a broad choice of parameters, these models have the standard universal α-attractor predictions [50–54] matching the Planck/BICEP/Keck Array data [41, 42]. In particular, $n_s = 1 - \frac{2}{N} \sim 0.96$–$0.97$ for the exponential attractors, where N is the number of e-foldings [52]. However, in the large uplift limit $V_{\mathrm{uplift}} \gg \frac{m^2}{2}\phi^2$ these models have another attractor regime, with $n_s = 1$. By changing the parameters, one can continuously interpolate between the two attractor predictions, $n_s = 1 - \frac{2}{N}$ and $n_s = 1$ [35]. Because of the double attractor structure of such models, their predictions are compatible with all presently available cosmological data. In the models where the tachyonic mass of the field χ at $\phi \lesssim \phi_c$ is smaller than the Hubble constant H, which we will study in this paper, the range of possible values of n_s is even broader.

In this paper, we will study the simplest versions of such models, explain how one can solve the problem of initial conditions there, and evaluate the spectrum of perturbations in these models. We will demonstrate that one can keep n_s and r consistent with the latest CMB data, while simultaneously controlling the shape, the width and the height of the peak of the spectrum of perturbations which determine the features of the PBHs and the stochastic SGWB background produced in this scenario.

This paper is organized as follows. We start with a discussion of hybrid inflation in the context of α-attractors in section 2. After reviewing the basic results of [35], we discuss the problem of initial conditions in our model in section 3. In section 4, we will make a step back and study the perturbations in the χ-sector of hybrid inflation, temporarily ignoring the field φ. As we will see, this will help to understand the origin of the high peak of perturbations produced in various versions of the hybrid inflation scenario. In section 5, we explain in details how the model parameters control distinct properties of the bump in the PPS and discuss the constraints from Planck/BICEP/Keck Array data. Then, in section 6, we describe the gravitational wave phenomenology of our model providing clear targets for gravitational wave interferometers and discussing how to interpret a future detection of a SGWB in terms of our model parameters. In section 7 we will generalize our results by considering models based on polynomial attractors or KKLTI potentials [54]. We conclude in section 8. In the appendix A, we provide an implementation of our model in SUGRA constructions. We set $M_{\mathrm{pl}} = 1$ throughout our analysis. The numerical results in this paper are obtained using a multifield extension of the BINGO code [55], presented in [56], which is however not yet public.

2 Hybrid α-attractors

Before describing the hybrid attractors [35], we will represent the original model (1.1), together with a small additional linear term $\mu^3\chi$, in a slightly different form, which is more convenient for our investigation:[1]

$$V(\chi, \phi) = M^2 \left[\frac{(\chi^2 - \chi_0^2)^2}{4\chi_0^2} + \frac{\tilde{m}^2}{2}\phi^2 + \frac{\tilde{g}^2}{2}\phi^2\chi^2 + d\,\chi \right]. \tag{2.1}$$

Here $\tilde{m} = m/M$, $\tilde{g} = g/M$, and $d = \frac{\mu^3}{M^2}$. In this paper we will consider models with $\chi_0 = O(1)$ and $\mu \sim M \sim m \sim g \sim 10^{-5}$, with masses given in the Planck mass units $M_{\mathrm{pl}} = 1$. In that

---

[1]One should also add a tiny constant term $\Delta V \approx -\mu^3\chi_0$ to the potential (2.1) to ensure nearly vanishing value of the cosmological constant, but it can be ignored in the discussion of inflation.

case $\tilde{m} \sim \tilde{g} = O(1)$, whereas the linear term can be very small, with $d \sim 10^{-5}$. Therefore it does not affect early stages of inflation. However, as we will see, it plays an important role in the theory of the PBH production.

Note that the linear term slightly breaks the symmetry $\chi \rightarrow -\chi$ of the original hybrid inflation scenario. This symmetry was introduced in [2, 3] for simplicity, it is not a fundamental requirement, and in our context there is no gauge symmetry protecting it. Thus one may argue that it is technically natural. Its possible interpretation in the context of supergravity is discussed in the appendix A.

In the original version of the hybrid inflation [2, 3], both ϕ and χ are canonically normalized. To present the simplest α-attractor generalization of the original model, it is sufficient to modify the kinetic term of the field ϕ:

$$\frac{\mathcal{L}}{\sqrt{-g}} = \frac{R}{2} - \frac{(\partial_\mu \phi)^2}{2\left(1 - \frac{\phi^2}{6\alpha}\right)^2} - \frac{(\partial_\mu \chi)^2}{2} - V(\chi, \phi). \tag{2.2}$$

One may also make a similar generalization of the kinetic term of the field χ [35], but it is not required in the context of our investigation. The geometric interpretation of this modification can be found in [57] and its supergravity implementation for hybrid attractors is given in [35] and in the appendix A of our paper.

Upon a transformation to the canonical variable φ, the hybrid inflation potential becomes

$$V(\chi, \varphi) = M^2 \left[\frac{(\chi^2 - \chi_0^2)^2}{4\chi_0^2} + 3\alpha(\tilde{m}^2 + \tilde{g}^2 \chi^2) \tanh^2 \frac{\varphi}{\sqrt{6\alpha}} + d\,\chi \right]. \tag{2.3}$$

The potential at $\chi = 0$ is given by

$$V(\varphi) = M^2 \left(\frac{\chi_0^2}{4} + 3\tilde{m}^2 \alpha \tanh^2 \frac{\varphi}{\sqrt{6\alpha}} \right). \tag{2.4}$$

This is the simplest α-attractor potential [50–54], uplifted by the term $V_{\text{uplift}} = \frac{M^2 \chi_0^2}{4}$. Another important parameter is the mass squared of the field χ at $\chi = 0$,

$$M_\chi^2 = V_{\chi,\chi}(\chi = 0) = M^2 \left(-1 + 6\alpha \tilde{g}^2 \tanh^2 \frac{\varphi}{\sqrt{6\alpha}} \right). \tag{2.5}$$

The last term in this equation stabilizes the inflationary trajectory $\chi = 0$ at large φ.

In this paper, we will consider the case $6\alpha \tilde{g}^2 > 1$. In that case $M_\chi^2 > 0$ at sufficiently large $\varphi > \varphi_c$, where

$$\tanh^2 \frac{\varphi_c}{\sqrt{6\alpha}} = \frac{1}{6\alpha \tilde{g}^2}. \tag{2.6}$$

During inflation, when the field φ decreases below φ_c, the mass squared of the field χ becomes negative and the tachyonic instability with generation of the scalar field χ develops. At $\varphi = 0$ this mass has its largest absolute value, $M_\chi^2(\varphi = 0) = -M^2$.

The potential (2.3) for some particular values of parameters is shown in figure 1.

It is instructive to compare $M_\chi^2(\varphi = 0) = -M^2$ with the Hubble constant at $\varphi = 0$,

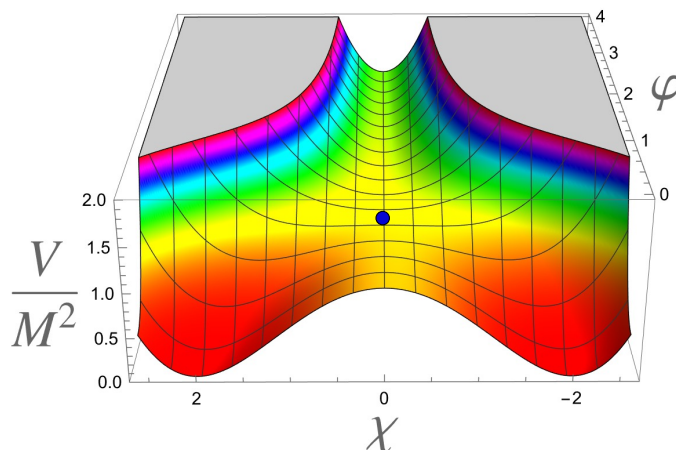$$H_0 = \sqrt{\frac{V_{\text{uplift}}}{3}} = \frac{M\chi_0}{2\sqrt{3}}. \tag{2.7}$$

Figure 1. Hybrid inflation potential for the model (2.3) with $\tilde{m} = 1/3, \chi_0 = 2, \tilde{g} = 1, \alpha = 1, d = -5 \times 10^{-6}$. The blue dot corresponds to φ_c (2.6), below which the mass of the field χ becomes tachyonic. Note that the effects of the linear term are almost invisible by eye.

The main regime explored in the original formulation of the hybrid inflation scenario was $\chi_0 \ll 1$ [2, 3], in which case the absolute value of the tachyonic mass M_χ becomes much larger than the Hubble constant as soon as ϕ becomes smaller than ϕ_c. This leads to an abrupt termination of inflation at $\phi \approx \phi_c$ [2, 3, 35].

In this paper, following [1], we will be interested in the opposite regime $\chi_0 \gtrsim 2\sqrt{3}$. In this regime $|M_\chi(\chi = 0)| \lesssim H$ for all $\varphi < \chi \lesssim \varphi_c$. This mass vanishes when the field φ is close to φ_c. As a result, the tachyonic instability is very slow to develop. Importantly, at any nonzero value of φ, its contribution to the equation of motion of the field χ is only slowing it down, and at $\varphi \ll \varphi_c$ the contribution of the field φ to the equation of motion of the field χ becomes negligible.

That is why one can learn quite a lot about the waterfall regime in such models by studying the evolution of the field χ from the top of the single-field inflationary potential $V(\chi) = (\chi^2 - \chi_0^2)^2 M^2 / 4\chi_0^2$, ignoring the field φ. We will discuss it in section 4. This will explain in an intuitive way why it is natural to expect a very high peak for the inflationary perturbations in such models, and how one can control its height. In subsequent sections, we will return to the full scenario describing classical and quantum evolution of both fields.

But before doing it, we will discuss the problem of initial conditions in this scenario. And the first question is: how did the scalar fields found their way into the narrow infinitely long valley with $\chi = 0$?

3   Initial conditions for inflation

As we can see from equation (2.1), the potential $V(\chi, \varphi)$ at $\varphi \gg \sqrt{6\alpha}$ practically does not depend on φ because in this regime the function $\tanh \frac{\varphi_c}{\sqrt{6\alpha}}$ becomes exponentially close to 1:

$$V(\chi, \varphi) \approx M^2 \left[\frac{(\chi^2 - \chi_0^2)^2}{4\chi_0^2} + 3\alpha(\tilde{m}^2 + \tilde{g}^2\chi^2) + d\,\chi \right]. \tag{3.1}$$

Thus at large φ one can apply to this theory the standard arguments of the single field chaotic inflation scenario [58–60]. One can consider a tiny Planck size domain of the universe with

the Planckian value of the potential energy of the field χ, and let it fall. If the kinetic and gradient energy of the fields initially are smaller that its potential energy, each such tiny domain becomes exponentially expanding.

The potential $V(\chi, \varphi)$ approaches the Planck boundary at $\chi^2 \sim 2\chi_0/M \gg 1$ for any value of φ in the infinitely large range $-\infty < \varphi < +\infty$. Therefore in this context it is natural to consider initial conditions where both fields are extremely large, but $\varphi \gg \chi$. For most of such initial conditions the field χ gradually falls down to the valley, oscillates with a rapidly decreasing amplitude, and relaxes at the bottom of the valley, and, only after that, the field φ begins to move towards $\varphi = 0$.

Note that, because of the tiny linear term $d\chi$, the field χ does not relax at $\chi = 0$, but it is slightly displaced in the direction depending on the sign of the coefficient d. At $\chi \ll \chi_0$ and $d \neq 0$ the valley is at the minimum of the potential

$$V(\chi, \varphi) \approx M^2 \left[\frac{1}{2} \left(-1 + 6\alpha \tilde{g}^2 \tanh^2 \frac{\varphi}{\sqrt{6\alpha}} \right) \chi^2 + d\chi \right] . \tag{3.2}$$

This potential admits an attractor for χ defined by its minimum at

$$\chi_{\text{attr}} = -\frac{d}{6\alpha \tilde{g}^2 \tanh^2 \frac{\varphi}{\sqrt{6\alpha}} - 1} . \tag{3.3}$$

As mentioned in the previous section, we study models with $6\alpha \tilde{g}^2 > 1$. At $\varphi \gg \sqrt{6\alpha}$, we have $\tanh^2 \varphi/\sqrt{6\alpha} \simeq 1$ and the minimum with respect to χ is at a constant φ-independent distance from $\chi = 0$:

$$\chi = -\frac{d}{6\alpha \tilde{g}^2 - 1} . \tag{3.4}$$

Because of the rapid decrease of the kinetic energy of the field χ during inflation, the amplitude of its oscillations about this minimum decreases exponentially fast. Then, the field φ starts slowly moving towards its smaller values, see figure 2. At $\sqrt{6\alpha} \gtrsim \varphi > \varphi_c$, the minimum of this potential moves further away from zero. Close to $\varphi = \varphi_c$, the part of the potential $\sim \chi^2$ vanishes, so it can no longer protect the field χ from growing due to the linear term $d\chi$.

Thus, even though this term $d\chi$ is very small, it pushes the field χ away from the $\chi = 0$. Eventually, the fields falls down to one of the two minima at $|\chi| \approx \chi_0$ at $\varphi = 0$. The choice of the minimum is completely independent on the initial conditions on the two fields, and rather depends on the sign of the coefficient d of the tiny linear term.

A more important statement is that if the initial values of the field φ are sufficiently large, the original oscillations of the field χ becomes exponentially damped, and the final results of our calculations of the spectrum of perturbations do not depend on initial conditions.

Simplicity and robustness of this process is one of the advantages of the original hybrid inflation scenario, as well as of its α-attractor generalization. Its most important part is the existence of a long valley to which the field χ falls, and the positive slope of the potential with respect to the field φ which pushes it along the valley towards $\varphi = 0$ [2, 61, 62].

The situation can be very different if one attempts to make the parameter m^2 negative, as in the toy model described in [44]. In that case, if one considers small initial values of the field ϕ, the field moves to $\phi = 0$, but without a significant fine-tuning of initial conditions it is difficult to achieve a long hybrid inflation regime starting with large χ, see figure 3. On the other hand, if one considers large initial values of ϕ, the field ϕ initially moves to smaller ϕ, but then it turns and rolls down along the valley towards very large ϕ with $V(\phi) < 0$,
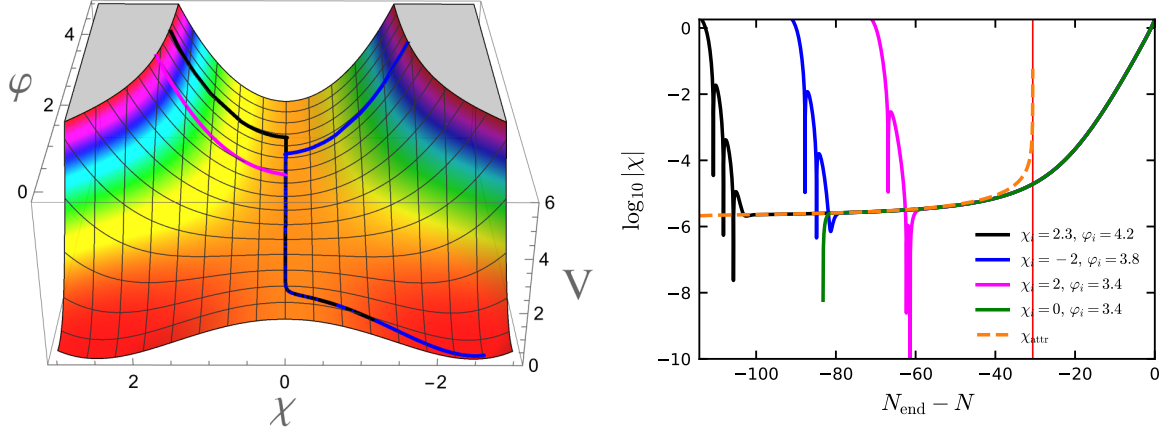
Figure 2. [Left] Initial conditions for hybrid attractors. The parameters used are those in section 5, eq. (5.1). The potential is shown in units of M^2. The fields begin at large values of φ and χ. Then χ rapidly falls down, and, after that, inflation driven by the field φ begins. Eventually, after φ crosses φ_c the field χ falls to one of the two minima of the potential $\chi \approx \pm\chi_0$ depending on the sign of d. The initial conditions are shown on the right panel. [Right] Evolution of the field χ for different initial conditions compared to the attractor solution in eq. (3.3). The agreement of the attractor solution with the numerical (exact) solution of χ is remarkable. As expected, it starts to deviate from the position of the minimum of the potential (3.3) close to when $\varphi \sim \varphi_c$. The power spectrum is clearly unaffected by the initial conditions.
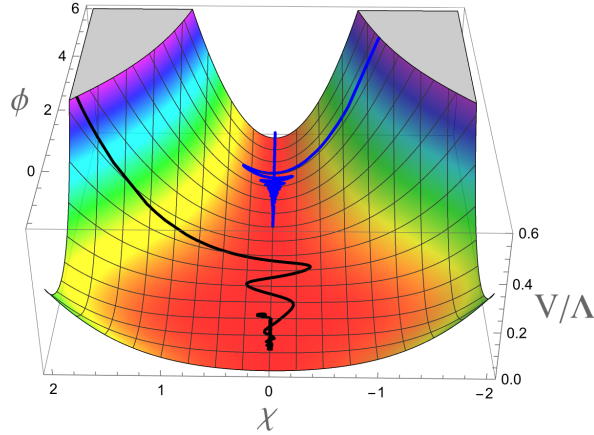

Figure 3. Initial conditions problem for the model (1) of ref. [44]. If evolution begins at smaller values of ϕ, as shown by the black line, the field evolution is chaotic, and hybrid inflation regime typically does not emerge. If evolution begins at greater values of ϕ, as shown by the blue line, the field ϕ turns, runs to infinity, its tachyonic potential becomes negative, and the universe collapses. In this example, we use the parameters of figure 3 in ref. [44] with $\phi_c = 0.1$ and $(\phi_i, \chi_i) = (3, 3), (4, -2)$ for the black and blue lines respectively.

and the universe collapses. It is possible to solve this problem by a proper modification of the potential used in [44] at $\phi > \phi_c$. Fortunately, this issue does not appear in the original version of the hybrid inflation scenario [2, 3], and in the hybrid attractor models described in our paper.

4 Evolution of the field χ in the single-field approximation

As we have argued in section 2, one can learn quite a lot about the waterfall stage of inflation in hybrid inflation with $\chi_0 \gtrsim 2\sqrt{3}$ by ignoring the field φ and investigating the single field model with

$$V(\chi) = \frac{M^2}{4\chi_0^2}(\chi^2 - \chi_0^2)^2 \,. \tag{4.1}$$

Many of our results will be valid for any single field inflationary potential; they will be based on the general theory of eternal inflation [63–66] which we will remind here following the general theory of eternal inflation developed in [66].

In the slow-roll approximation, ignoring quantum fluctuations, during each e-folding the scalar field decreases by

$$\Delta\chi = \frac{V_\chi}{V} \,, \tag{4.2}$$

where $V_\chi = \frac{\partial V}{\partial \chi}$. During that time the volume of each inflationary domain of the horizon size $\mathcal{O}(H^{-1})$ increases $e^3 \sim 20$ times, so we get ~ 20 independent horizon-size inflationary domains where the average value of the field χ decreases by $\Delta\chi = V_\chi/V$.

However, during the same time, inflationary quantum fluctuations may increase the value of χ by

$$\delta\chi \sim \frac{H}{2\pi} = \frac{\sqrt{V}}{2\sqrt{3}\,\pi} \,. \tag{4.3}$$

If $\delta\chi > |\Delta\chi|$, these quantum jumps may bring half of the 20 horizon-size domain uphill, back to where we started. This leads to the regime of eternal inflation [66]. Remarkably, as one can easily see, the condition $\delta\chi < |\Delta\chi|$ required for the absence of eternal inflation is equivalent to the condition that the amplitude of perturbations is smaller than $\mathcal{O}(1)$:

$$A_s = \frac{V^3}{12\pi^2 V_\chi^2} \lesssim 1. \tag{4.4}$$

This is not a coincidence, since eternal inflation would imply that inflation continues in some parts of the universe, whereas in many other parts of the universe inflation is over and the energy density rapidly becomes small.

In the context of the model (4.1), the criterion (4.4) is always violated at the top of the potential where $V_\chi \sim 0$. However, quantum fluctuations in each horizon size domain during one e-folding of inflation shift the field χ from $\chi = 0$ by $\delta\chi \sim \frac{H}{2\pi}$. Thus one can use this estimate for the initial beginning of the inflationary trajectory. Expanding $V(\chi) = V + V_{\chi,\chi}\chi^2/2$ we find a simple criterion for the existence of eternal inflation at the top of the potential: $|V_{\chi,\chi}| \lesssim V$.

A similar and perhaps a slightly more accurate estimate can be obtained by investigation of eternally inflating domain walls separating parts of the universe with $\chi > 0$ from the parts with $\chi < 0$ [67–69]. According to [70], this happens for

$$\frac{|V_{\chi,\chi}|}{V} < \frac{9}{2\pi} \,. \tag{4.5}$$

This means that if this slow-roll condition is satisfied at the top of the potential, inflation there is eternal.

In application to the model (4.1), eternally inflating topological domain walls appear if

$$M \lesssim 2H\,, \tag{4.6}$$

or, equivalently, if [70]

$$\chi_0 \gtrsim 1.7\,. \tag{4.7}$$

What relation does it have to the two-field evolution in the hybrid inflation scenario? The answer is that if the field φ initially was large, during the long process of its rolling along the valley of the potential at $\varphi > \varphi_c$ any original oscillations of the field χ disappear, and it becomes stabilized at $\chi = 0$. Then when the field φ passes the critical point φ_c, the field χ may start falling down. Since $V_\chi = 0$ at $\chi = 0$, the field χ can fall down from $\chi = 0$ only due to generation of inflationary perturbations.

Note that while the field φ rolls to $\varphi = 0$, the Hubble constant decreases, whereas the absolute value of the tachyonic mass squared $|M_\chi^2|$ increases until it reaches M^2. Therefore if the condition (4.5), (4.6) is satisfied at $\varphi = 0$, it is satisfied everywhere along the ridge $\chi = 0$, $\varphi < \varphi_c$. In that case we enter the eternal inflation regime, the process which generates enormous density perturbations on the scale well within the observable part of the universe. There perturbations are sufficient for producing not only PBH, but also eternally inflating domain walls separating parts of the universe with $\chi > 0$ from the parts with $\chi < 0$.

Thus the first conclusion which follows from this analysis is that in hybrid inflation with $M \lesssim H$ it is very easy to produce PBH. The only problem here is how to avoid overproducing PBH and inflating topological defects.

The simplest way to avoid eternal inflation and to decrease the amplitude of perturbations below $O(1)$ is to consider models with $\chi_0 \ll 1$. It is still possible to have a second stage of fast roll inflation in this scenario, producing large perturbations [1, 44, 71]. However, this does not address the problem of superheavy topological defects in such models.

To solve both problems simultaneously, we added the small term $\mu^3 \chi$ to the potential (2.1), see (3.1). In that case one has $V_\chi(\chi = 0, \varphi = 0) = \mu^3$, and the condition $A_s < 1$ reads

$$\mu^3 \gtrsim \frac{V^{3/2}}{2\sqrt{3}\pi}\,. \tag{4.8}$$

To give a particular example, for $V \sim 10^{-10}$ this condition implies that $\mu^3 \gtrsim 10^{-16}$. This means that by adding a tiny term $10^{-16}\chi$ to the potential one can avoid the problems discussed above. The corresponding constraint on $d = \mu^3/M^2$ is

$$d \gtrsim \frac{M\chi_0^3}{2^4\sqrt{3}\pi}\,. \tag{4.9}$$

As we mentioned in section 3, the term $d\,\chi$ leads to an additional modification of this scenario. In its absence, the field χ is rolling along the minimum of the potential at $\chi = 0$, which is why in our previous estimates of the amplitude of the perturbations we used $\chi = 0$ as a starting point of the inflationary waterfall. However, the term $d\,\chi$ pushes the field χ slightly away from $\chi = 0$. This happens well before φ becomes smaller than φ_c, see (3.4), (3.3). Thus, even though the linear term $d\,\chi$ is very small, it pushes the field χ away from the ridge of the potential and from its initial equilibrium state (3.3). This additionally decreases the height of the peak of the perturbations. On the other hand, during the several e-foldings near φ_c the average amplitude of the perturbations may grow slightly above $\frac{H}{2\pi}$, by a factor $O(1)$. Therefore it

would be interesting to perform a more detailed investigation of stochastic effects during inflation, following [72–83]. However, we believe that the simple estimates (4.8), (4.9) give a good estimate of the range of validity of the perturbative analysis to be used in this paper.

Thus we see that by adding the term $d\chi$ to the potential, one can control the height of the peak of the perturbations. A detailed analysis of the perturbations produced in the full two-field scenario is rather sophisticated and will be given in the next section. Interestingly, we will find that the spectrum of the perturbations produced at φ sufficiently far below the critical point φ_c is well described by the theory of perturbations in the single-field model described in this section, while around the critical point φ_c multifield effects play a non-negligible role.

5 Hybrid exponential attractors and the spectrum of perturbations

In this section we will perform a full numerical investigation of perturbations in hybrid attractors. For illustration, we will consider the exponential attractor model in eq. (2.1) and consider the following combination of parameters as a benchmark

$$M = 1.47 \times 10^{-5}\,, \quad \alpha = 1\,, \quad \tilde{g} = 0.8\,, \quad \tilde{m} = 0.3\,, \quad \chi_0 = 2.5\,, \ d = -5 \times 10^{-6}\,, \qquad (5.1)$$

which we denote as the *baseline* parameters and explore how changing each parameter affects the shape and amplitude of the bump in the primordial power spectrum that is produced at small scales. Note that we always set the field χ initially at rest at $\chi_i = 0$ and we adopt the initial condition $\varphi_i = 3.4$, which corresponds to 83 e-folds of inflation. The trajectory is shown in the left panel of figure 4. Our baseline parameters in eq. (5.1) are chosen so that

$$\ln 10^{10} A_s = 3.043\,, \quad n_s = 0.9618\,, \quad \alpha_s = 3.1 \times 10^{-6}\,, \quad r_{0.002\,\mathrm{Mpc}^{-1}} = 0.01\,, \qquad (5.2)$$

well consistent with Planck/BICEP/Keck Array latest constraints at large scales. Note that the amplitude $\ln 10^{10} A_s$, the tilt n_s and the running of the tilt α_s are computed at the pivot scale $k_* = 0.05\,\mathrm{Mpc}^{-1}$ assuming that it crosses the Hubble radius $N_* = 55$ e-folds before the end of inflation.[2] Changing some of the parameters in (5.1) also slightly affects predictions at CMB scales. This effect can always be counterbalanced by tweaking more parameters at the same time.

We note that recent efforts to solve the so-called H_0 *tension* require a reinterpretation of available data, which, taken at face value, would imply higher values of n_s, all the way up to $n_s = 1$, i.e. the Harrison-Zeldovich value [84–87]. While it is not our goal to discuss such claims, we show at the end of this section that we can easily obtain larger values of n_s in our model.

We will also consider another example described by the parameters:

$$M = 9.48 \times 10^{-6}\,, \quad \alpha = 1\,, \quad \tilde{g} = 1\,, \quad \tilde{m} = 1\,, \quad \chi_0 = 2.58\,, \ d = -10^{-5}\,. \qquad (5.3)$$

Its trajectory is shown in the right panel of figure 4. As can be seen, compared to the baseline model, the hybrid field starts to move only when φ has approached $\varphi \simeq 0$. While this example has a spectral index which is too red to fit Planck data, the waterfall phase here is closer to a single-field stage of inflation, so it is useful for illustrative purposes and to be compared to the intuitive arguments presented in the previous section.

---

[2]N_* is affected by uncertainties that comes from our incomplete understanding of reheating. Clearly a larger/smaller N_* would shift the peak in the power spectrum towards smaller/larger scales and give a bluer/redder n_s compared to what we report in the main text.
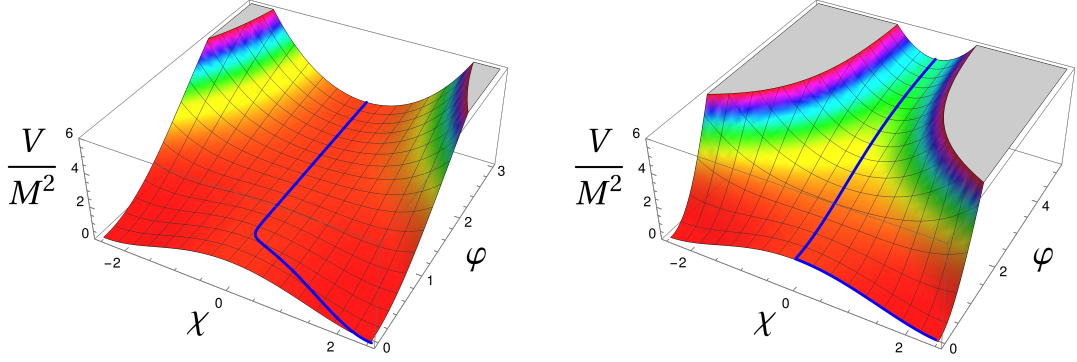
Figure 4. Trajectory in the exponential attractor model for the baseline parameters in eq. (5.1) (left) and for the parameters in eq. (5.3) (right). To better appreciate the differences, we set the same range for the y-axis.

Let us briefly summarize here the mechanism that leads to a peak in $\mathcal{P}(k)$, also anticipated in the previous sections, from the perspective of the full multifield dynamics. The piece of the trajectory producing the perturbations at the CMB scales consists in a simple slow-roll phase along the φ direction. During this stage, the field χ slowly increases due to the linear term. Inflation is dominated by the slowly-rolling inflaton φ and curvature perturbations do not experience amplification. Eventually, when φ crosses the critical value φ_c, the effective mass squared of the field χ becomes negative, it develops an instability and isocurvature perturbations start to grow exponentially.

Even during this period, however, curvature perturbations experience the usual evolution and freeze to a constant value after Hubble crossing. The trajectory turns and the field χ rolls towards the minimum of the potential at χ_0, taking a few e-folds to terminate inflation. At the moment of the turn, the coupling between curvature and isocurvature perturbations is switched on and power in the latter is quickly transferred to the former, leading to a large peak in the PPS. We emphasize that the sourcing entirely occurs on super-Hubble scales, as opposed to recently proposed models where the turn sources amplification around Hubble crossing [6–11]. It is also important to understand that, while isocurvature perturbations do grow during inflation, almost all of the power is transferred to the curvature ones during the turn, leaving the spectrum of primordial perturbations after inflation adiabatic, consistently with tight bounds on primordial isocurvature from CMB data [41].

To understand this process, it is useful to investigate the behavior of two important quantities, i.e. the effective mass squared of isocurvature modes on superhorizon scales:[3]

$$\frac{m^2_{\text{eff, iso}}}{H^2} = \frac{1}{(\dot{\varphi}^2 + \dot{\chi}^2)\, H^2} \left[V_{\varphi\varphi}\, \dot{\chi}^2 - 2V_{\chi\varphi}\, \dot{\varphi}\dot{\chi} + V_{\chi\chi}\, \dot{\varphi}^2 \right] + 3\eta_\perp^2, \tag{5.4}$$

which describes the exponential growth of isocurvature modes, and the turn rate

$$\eta_\perp^2 = \frac{1}{(\dot{\varphi}^2 + \dot{\chi}^2)\, H^2} \left[V_\varphi\, \dot{\chi} - V_\chi\, \dot{\varphi} \right]^2, \tag{5.5}$$

---

[3]We note that sometimes the quantity $m^2_{\text{iso}}/H^2 = m^2_{\text{eff, iso}}/H^2 - 4\eta_\perp^2$ is also discussed in the literature. The two quantities are conceptually different as $m^2_{\text{eff, iso}}/H^2$ is the *effective* mass squared of isocurvature perturbations obtained integrating out the evolution of curvature perturbations on super-horizon scales, while m^2_{iso}/H^2 really corresponds to the mass of isocurvature perturbations. However, in hybrid inflation, most of the growth of isocurvature perturbations occurs *before* the turn, when $\eta_\perp^2 \simeq 0$ and the two quantities are numerically equivalent.
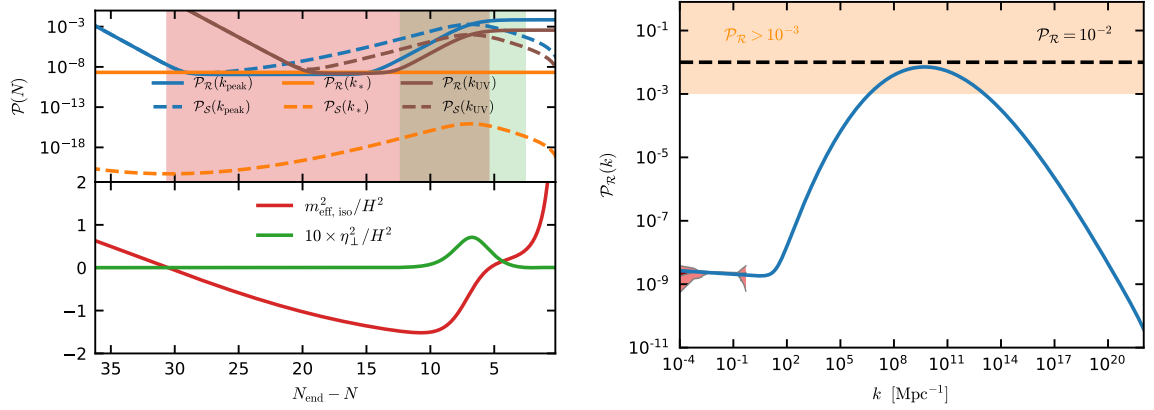
Figure 5. [Left] Time evolution of the dimensionless spectra of curvature and isocurvature perturbations in the baseline case. We show the evolution for the peak scale $k_{\rm peak} \simeq 5.3 \times 10^9 \, {\rm Mpc}^{-1}$ and, for a comparison, the pivot scale $k_* = 0.05 \, {\rm Mpc}^{-1}$ and a smaller-scale mode $k_{\rm UV} = 10^{14} \, {\rm Mpc}^{-1}$. Green and red areas correspond to the regions where $\eta_\perp^2/H^2 > 10^{-2}$ and $m_{\rm eff, \, iso}^2/H^2 < 0$ respectively, as shown in the lower part of the plot. [Right] PPS at the end of inflation. The yellow-shaded area is the region $\mathcal{P}_\mathcal{R}(k) \gtrsim 10^{-3}$ where we expect a sizable production of PBHs. The dashed black line is $\mathcal{P}_\mathcal{R} = 0.01$, which is the value commonly used as criterium for PBH formation. The parameters used to produce this figure are the baseline parameters in (5.1).

which controls the coupling between curvature and isocurvature modes and the resulting amplification of the former.

These quantities are plotted in the left panel of figure 5, together with the evolution of the dimensionless spectra of curvature $\mathcal{R}_k$ and isocurvature perturbations $\mathcal{S}_k$ for some illustrative wavenumbers k. As can be seen, as soon as φ crosses φ_c and $m_{\rm eff, \, iso}^2/H^2$ becomes negative, isocurvature perturbations start to grow. This amplification is experienced by *all* the modes, however, since $m_{\rm eff, \, iso}^2/H^2 > 0$ for $\varphi > \varphi_c$, isocurvature modes which cross the Hubble radius long before the instability decay before have sufficiently decayed so that their amplitude is too small to source curvature perturbations, even if they get amplified (see dashed orange line in the left panel of figure 5). Note that isocurvature modes that cross the horizon later than the peak scale and are still sub-horizon at $\varphi = \varphi_c$) have less time to grow, resulting in a smaller amplification of curvature modes during the turn (see brown lines in figure 5). Very small scale modes cross the horizon long after the turn, when inflation is completely driven by χ, and their evolution is just the typical slow-roll one, with isocurvature perturbations decaying straight after horizon crossing.

The net effect of such amplification is to produce a broad bump in the PPS. If the amplitude of the bump is large enough, the perturbations can collapse into PBHs when they re-enter the Hubble radius during radiation dominated era [1]. The criterium for PBHs to form is very sensitive to many assumptions, and it is not the purpose of this paper to study it in details. Nevertheless, it generically requires $\mathcal{P}_\mathcal{R} \gtrsim 10^{-3} - 10^{-2}$ (see e.g. refs. [34, 88, 89]) as indicated by the yellow shaded area in the right panel of figure 5. This can easily be satisfied by our model.

The next issue to consider in the masses of PBH formed after inflation. This is a rather complicated story, we will limit ourselves to simple estimates. Consider perturbations produced at the peak, $\Delta N = N_{\rm end} - N_{\rm peak}$ e-foldings from the end of inflation. The mass of PBH can be estimated by the total energy inside the horizon when these perturbations

re-enter the horizon. If the evolution until that time was matter dominated (which happens if reheating is very inefficient), then one can roughly estimate $M_{\mathrm{PBH}} \sim O(10)\, H^{-1} e^{3\Delta N}$, in Planck mass units, where H is the Hubble constant at the end of inflation. For a radiation dominated universe (efficient reheating) the masses are expected to be much smaller, $M_{\mathrm{PBH}} \sim O(10)\, H^{-1} e^{2\Delta N}$ [1, 90]. The reason for the smaller mass in the second case is the redshift of radiation, which occurs prior to the horizon re-enter. In more realistic situations, where the PBH formation occurs in a universe with $p = \rho/3$ after a long stage of matter domination, the redshift is less efficient, and one may expect M_{PBH} between the two limits discussed above [10, 17].

To give a particular example, consider the universe which was radiation dominated soon after the end of inflation. In this case one may use the expression that relates the scale of a perturbation to the mass of the formed PBH [91]:

$$\frac{M(k)}{M_\odot} \simeq 10^{-16} \left(\frac{\gamma}{0.2} \right) \left(\frac{g(T_k)}{106.75} \right)^{-1/6} \left(\frac{k}{10^{14}\,\mathrm{Mpc}^{-1}} \right)^{-2}, \tag{5.6}$$

where γ is a factor that encodes the efficiency of the collapse to PBHs and $g(T_k)$ is the effective number of relativistic degrees of freedom at the time (or, equivalently, temperature) of formation. For example, assuming $\gamma = 0.2$ and $g(T_k) = 106.75$, the baseline power spectrum would produce a PBH mass function peaked around $M \sim 10^{-8}\, M_\odot$. While this is excluded by microlensing experiments [89], we will shortly see that the parameters can be tuned to shift the location of the peak and give rise to much heavier or much lighter PBHs. For example, the green line in the top-right panel of figure 6 shows a peak at $k_{\mathrm{peak}} = 1.3 \times 10^{12}\,\mathrm{Mpc}^{-1}$, corresponding to PBHs of masses $M_{\mathrm{PBH}} \sim 6 \times 10^{-13}\, M_\odot$, that can constitute the totality of the Cold Dark Matter in our Universe [89]. Also note that the abundance of PBHs depends exponentially on ratio of the primordial power spectrum to the critical value of the density contrast δ_c, therefore, depending on the specific value adopted, the power spectrum shown in figure 5 could result in no PBHs to an overproduction of PBHs.

The bump-like shape of the power spectrum at small scales suggests that we can control properties such as its amplitude, location and width by choosing different combinations of the model parameters. Phenomenologically, this does not strongly impact the formation of PBHs, which, being a critical process, is mainly sensitive to the peak amplitude [92], so the relevant features are just its amplitude and location. However, the frequency profile has implications on the SGWB (see next section), which is sensitive to a wider portion of the bump. Therefore, we now analyze the effects of varying the model parameters and show our results in figure 6.

The parameter controlling the *amplitude of the peak* is the amplitude d of the linear term in the potential. Intuitively, this is very simple to understand. As we have shown in the previous section, in the absence of the linear term in the models with $\chi_0 \gtrsim 1.7$ one has eternal inflation at the ridge of the potential at $\chi = 0$, which results in $\mathcal{O}(1)$ perturbations. The term $d\,\chi$ moves us away from the eternal inflation regime, decreasing the amplitude in a controllable way. When the field φ moves sufficiently far away of the critical point φ_c, its equations of motion depend less and less on the field φ. Following the argument in the previous section, we would like to approximate the resulting amplitude of perturbations produced at this stage by the simple single-field equation (4.4). We illustrate it in figure 7.

As can be seen, the approximation is quite bad for the amplitude of the peak in the baseline example though it becomes reasonable for the spectrum away from the peak. This approximation becomes much better in the second example, shown in the right sides of figures 4, 7. The reason is that in the second example the turn is sharper and the waterfall
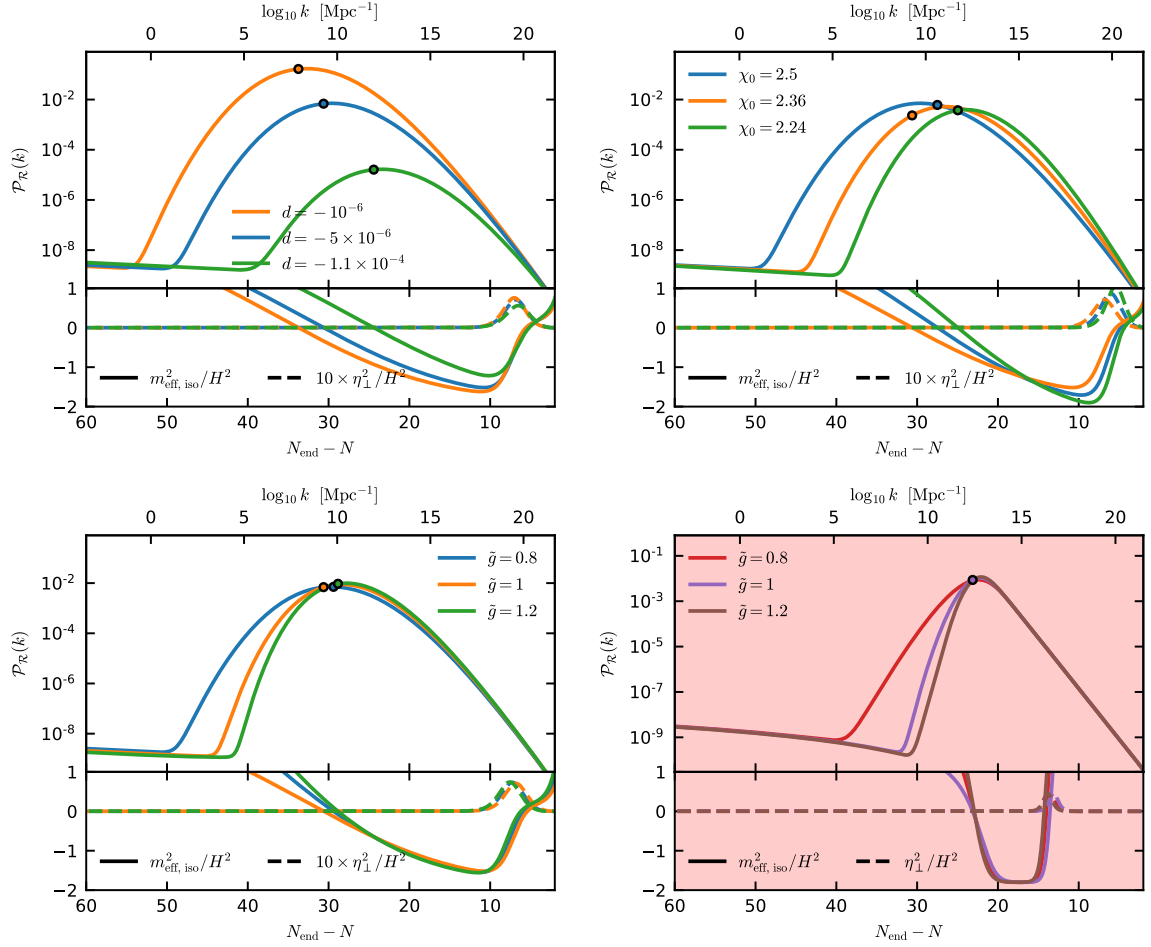
Figure 6. Variation of model parameters and their imprints on the PPS. For each case, we also plot the evolution of $m_{\text{eff, iso}}^2/H^2$ and $\eta_\perp^2/H^2$. [Top-left] Variation of d, which controls the height of the peak. [Top-right] Variation of χ_0, which controls the location of the peak. [Bottom-left] Variation of $\tilde{g}$, which controls the width of the peak. [Bottom-right] Variation of $\tilde{g}$ for the parameters in (5.3). To highlight that the last case is not compatible with Planck observations, we plot it on top of a red background (n_s is redder in that case). We also note that the x-scale axes on the bottom $N_{\text{end}} - N$ correspond to the time at which the wavenumbers on the top axes cross the horizon i.e. $k = a(N_{\text{end}} - N)H(N_{\text{end}} - N)$.

stage is entirely driven by χ, i.e. the trajectory is in the χ direction, with the field φ being approximately constant $\varphi \simeq 0$. Therefore, during the last ~ 10 e-folds after the turn with $\eta_\perp^2/H^2 \sim 0$, the numerical power spectrum matches well the slow-roll prediction $\mathcal{P}_\mathcal{R} \simeq V^3/12\pi^2 V_\chi^2 \simeq H^2/8\pi^2\epsilon$. On the other hand, in the baseline case the trajectory is still slowly turning close to the end of inflation, and the approximation to the single-field inflation driven by χ is rough.

We note that, though ϵ only becomes large close to the end of inflation, it does grow reasonably fast during the waterfall stage, so its logarithmic derivative, i.e. the second slow-roll parameter η is not negligible. Therefore the simple expressions $\mathcal{P}_\mathcal{R} \simeq V^3/12\pi^2 V_{\chi(\varphi)}^2 \simeq H^2/8\pi^2\epsilon$, which are derived at first order in slow-roll receive higher order corrections. In
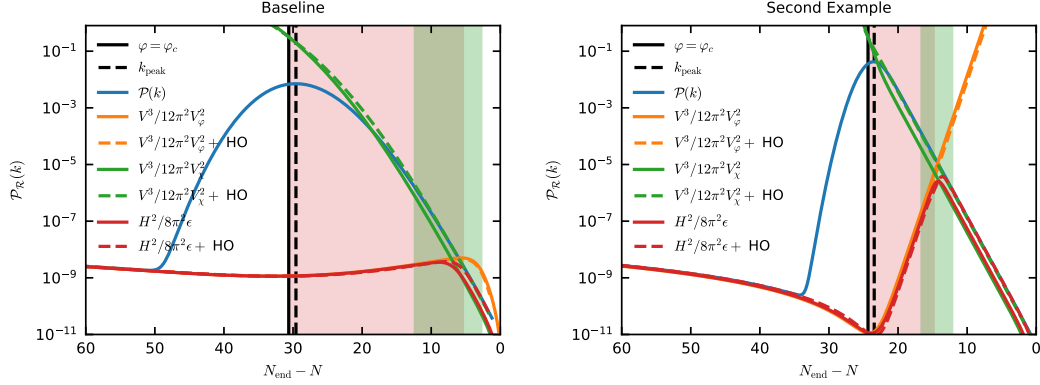
Figure 7. We compare the single-field slow-roll approximations for the primordial power spectrum to the exact numerical results for the baseline example in eq. (5.1) (left) and for the example in eq. (5.3) (right). Red and green regions have the same meaning as in figure 5.

particular, the expression for the spectrum at horizon crossing $k \sim aH$ becomes [93]:

$$\mathcal{P}_{\mathcal{R}} \simeq \frac{H^2}{8\pi^2\epsilon} \left[\frac{1}{\pi} \left(2 - 2\epsilon \right)^{2\nu-1} \Gamma^2(\nu) \right], \tag{5.7}$$

where $\nu = 1/2 + 1/(1 - \epsilon) + \eta/2$ and Γ is the Gamma function. Expressions for this quantity during the stages of inflation driven by φ or χ can be obtained by using $\epsilon \simeq \epsilon_V = \left(V_{\varphi(\chi)}/V \right)^2 / 2$ and $\eta \simeq 4\epsilon_V - 2\eta_V$, where $\eta_V = V_{\varphi\varphi(\chi\chi)}/V$, where ϕ_i denotes either χ, or ϕ, depending on which one drives inflation at a given stage.

As can be seen from the dashed lines in figure 7, the agreement on the spectrum produced after the peak is now much better and the formula correctly reproduces the power spectrum at the very small scales that cross the horizon when the slow-roll parameters are large and the hybrid field χ is ending inflation.

Another interesting feature that can be understood from figure 7 is that the peak in the power spectrum is very close to the scale that crosses the horizon when $\varphi = \varphi_c$, i.e. the one for which isocurvature perturbations experience the largest growth without having decayed on superhorizon scales prior to $\varphi = \varphi_c$. While, in the second example, we see from the plot that the amplitude of the spectrum at k_{peak} can be approximated quite well by $\mathcal{P}_{\mathcal{R}} \simeq V^3/12\pi^2 V_\chi^2$, we stress again, that this approximation is rigorous only after the turn, when inflation is effectively single-field, and that we must compute the full multifield dynamics to get exact results.

The *location of the peak* is controlled by the duration of the waterfall phase, which essentially depends on the χ_0 (see top-right panel of figure 6). Smaller values of χ_0 imply that the minimum in the χ direction is closer to $\chi \simeq 0$ and the waterfall stage is thus shorter. For this reason, the amplified modes cross the Hubble radius closer to the end of inflation and the peak in the power spectrum occurs at smaller scales (larger wavenumbers). Therefore, tuning χ_0, we can easily control the mass of the produced PBHs, which scales exponentially with N, i.e. $M \sim k^{-2} \sim e^{2(N_{\text{end}}-N_{\text{peak}})}$, see eq. (5.6). Clearly, shifting χ_0, we would need to adjust other parameters to maintain the consistency with large scale data, as explained below.

Finally, the coupling between the two fields χ and φ is responsible for the *width of the peak*. While the coupling does not change the stage with $m^2_{\text{eff, iso}}/H^2 < 0$, it significantly affects the evolution of $m^2_{\text{eff, iso}}/H^2$ at earlier times. In particular, a larger value of g makes the effective squared mass of isocurvature perturbations much larger for $\varphi > \varphi_c$. Therefore,

isocurvature modes that are super-horizon before the tachyonic instability decay very fast and their subsequent amplification is not enough to impact the evolution of curvature perturbations. On the other hand, modes that cross the Hubble radius after the tachyonic instability has developed are not affected by this. As such, the shape of the bump is only modified at scales $k < k_{\text{peak}}$ (see bottom-left panel of figure 6). This effect is particularly pronounced in the bottom-right panel, where we show the variation with $\tilde{g}$ for a different combination of parameters.

Armed with our understanding of the model parameters and their effects on the power spectrum, we would like to ask a final question. What is the relation of our results to the simple α-attractor prediction[4] $n_s = 1 - \frac{2}{N}$? Or, in other words, how much are we taking advantage of the attractor nature of the model?

As we will shortly discuss, these questions are partly related to the last parameter of the model, whose effects we have not explored so far, i.e. the parameter $\tilde{m}$, which controls the amplitude of the plateau at large values of φ relative to the uplift. We note that the following discussion can be straightforwardly generalized to *polynomial* attractors model that we construct in section 7, which have different attractor predictions, see e.g. eq. (7.4).

Let us first clarify the meaning of N in $n_s(N) = 1 - \frac{2}{N}$. In single-field α attractors models, N represents the number of e-folds from the moment at which the pivot scale crosses the Hubble radius to the end of inflation. Therefore, to be as clear as possible, the quantity we are interested is $n_s(N_*)$. As stressed above, we adopt $N_* = 55$ in our paper. More specifically, the attractor expression is derived by analytically solving the slow-roll equation for the inflaton $\varphi(N)$ as a function of N and plugging it into the slow-roll approximation for the spectral index $n_s \simeq 1 - 6\epsilon_V + 2\eta_V$.

However, in our model, where we have two stages of inflation, the equation for n_s needs to be modified as [10, 35]:

$$n_s = 1 - \frac{2}{N_* - \Delta N}. \tag{5.8}$$

This is very easy to understand, as the second stage shifts the end of inflation by ΔN. In this way, we relate the value of n_s to the region of the plateau that is producing the perturbations at N_*. However, how do we define ΔN? An intuitive way to do so would be to define it as the distance from the time where $\eta_{\perp}^2/H^2$ peaks, which roughly separates the region two stages of inflation driven φ and χ, to the end of inflation. However, in our model, there are situations where this is not the best definition for ΔN. Take the second example in figure 4. There, φ approaches 0 some e-folds after $\epsilon_\varphi = (V'/V)^2/2$ reaches its maximum, i.e. the point of maximum velocity of φ, and significantly slows down afterwards. However, since χ is moving very slowly and its kinetic energy is much smaller than that of φ, it takes roughly ~ 10 e-folds before $\eta_{\perp}^2/H^2$ peaks and the trajectory turns into the χ direction. This is different from what would happen in the single-field case, where inflation would end shortly after ϵ_φ reaches its maximum value, which in that context is $\epsilon_\varphi = 1$.

A more sensible definition, which resembles more the one single-field α-attractor model, is in fact to choose the time at which ϵ_φ peaks, so that $\Delta N \equiv N_{\epsilon_\varphi=\text{maximum}} - N_{\text{end}}$.[5] In this way, regardless of what happens after $N_{\epsilon_\varphi=\text{maximum}}$, eq. (5.8) should match quite well the prediction, as long as the first stage of inflation is independent from the first one. This, in turn depends mainly on the combination of parameters $\tilde{m}\sqrt{\alpha}$.

---

[4] We only consider the spectral index here for simplicity.

[5] We stress that this is ΔN is not the duration of the waterfall stage, which instead begins when $\varphi = \varphi_c$ and χ develops an instability.
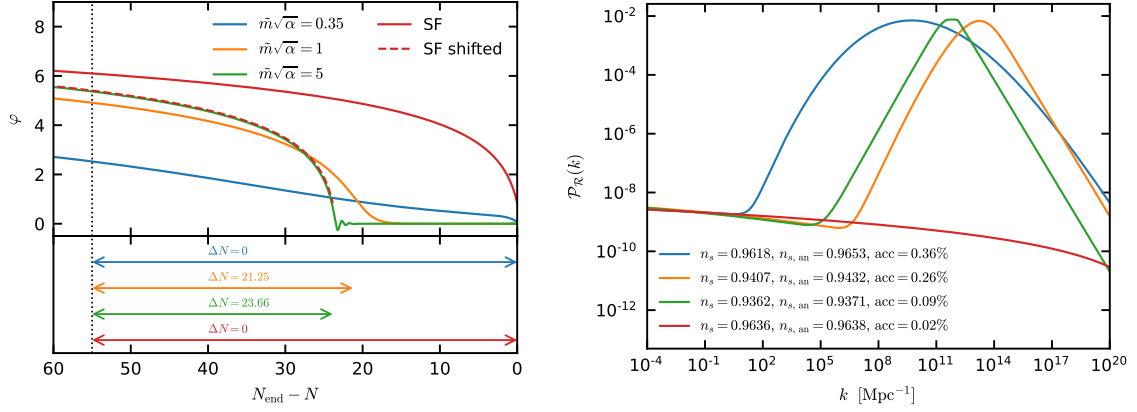
Figure 8. Varying $\tilde{m}$ and its effect on the field evolution (left) and the primordial power spectrum (right).

Also, note that, even after the modification $N_* \to N_* - \Delta N$ the simple eq. (5.8) would be adequate only if there was no uplifting potential. In that case, the equation needs to be further modified as:

$$n_s - 1 = 1 - \frac{2V_0\gamma^2}{V_0\gamma^2\left(N_* - \Delta N\right) + \left(V_{\mathrm{up}} + V_0\right)e^{\gamma s_c}}, \tag{5.9}$$

where $\gamma = \sqrt{2/3\alpha}$, $s_c = \varphi_c - \frac{1}{\gamma}\ln 4$, $V_0 = 3\alpha\tilde{m}^2M^2$ and $V_{\mathrm{up}} = M^2\chi_0^2/4$, see eq. (4.10) of ref. [35]. Note that eq. (5.9) reduces to eq. (5.8) if $V_{\mathrm{up}} + V_0 \ll V_0\gamma^2(N_* - \Delta N)e^{-\gamma s_0}$. On the other hand, in the large uplift limit $V_{\mathrm{up}} + V_0 \gg V_0\gamma^2(N_* - \Delta N)e^{-\gamma s_0}$ the value of n_s moves towards $n_s = 1$ [35].[6]

In figure 8, we show the sensitivity of our results to the parameter $\tilde{m}$. We plot the evolution of the field φ together with the corresponding primordial power spectra. The change in $\tilde{m}\sqrt{\alpha}$ is accompanied by a change in the initial condition φ_i to get the same number of e-folds in all the cases and by a change in the $d = -10^{-5}$ in the case with $\tilde{m}\sqrt{\alpha} = 1$ and $\tilde{g} = 2.5$ in the case with $\tilde{m}\sqrt{\alpha} = 5$, so that all the spectra show a peak of a comparable amplitude. α and χ_0 are kept fixed to the baseline values. For a comparison, we show in red the evolution of φ in the single-field α-attractor model.

As can be seen, the evolution for φ gets more and more similar to the corresponding single-field evolution as $\tilde{m}\sqrt{\alpha}$ increases, recovering the attractor predictions for large values of V_0/V_{up}. This is confirmed by the values of n_s reported in figure 8, which agree with eq. (5.9). Therefore, the conclusion is that, if we want to take advantage of the attractor predictions, we need a large V_0/V_{up}. In that case, however, for typical values of ΔN required to have interesting phenomenological effects at small scales, $n_s \sim 1 - 2/(N_* - \Delta N)$ is too red to fit Planck data.

Let us stress that this does not mean that our model is excluded by observations. In fact, as discussed above, the baseline example perfectly agrees with Planck measurements.

---

[6]Note that with an increase of V_{up} the attractor $n_s = 1$ may be reached twice. Indeed, when V_{up} increases, the evolution of the field φ slows down, so the last 55 e-foldings of inflation may happen at $\varphi < \sqrt{6\alpha}$, when the potential $\sim \tanh^2\frac{\varphi}{\sqrt{6\alpha}}$ is reduced to the original quadratic potential. In this case, with the growth of V_{up} the value of n_s crosses $n_s = 1$, continues to grow for a while, and then decreases and approaches its final attractor value $n_s = 1$. And with the account taken of the full two-field evolution, the situation becomes even more complicated, which is why we needed a detailed numerical analysis described in this section.
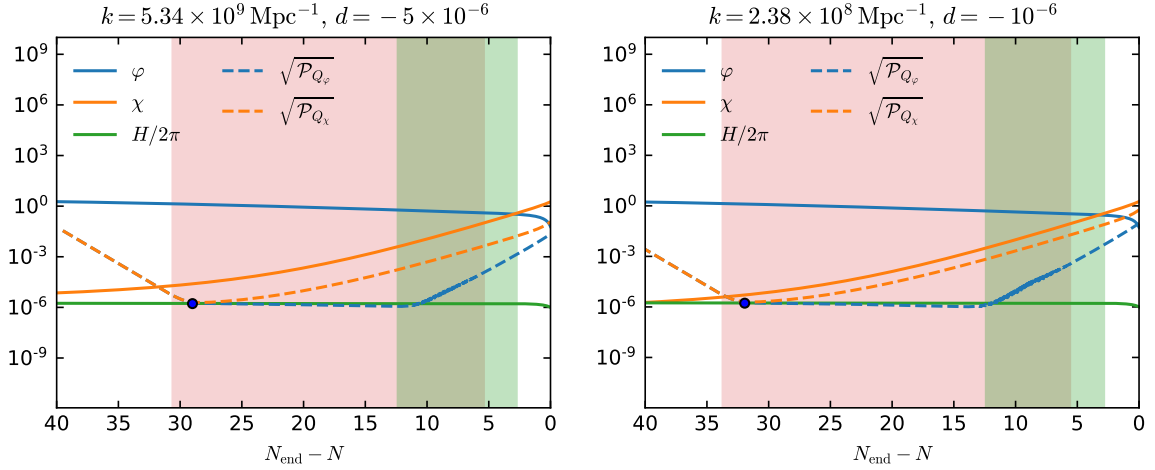
Figure 9. Evolution of perturbations for the cases shown in the top left panel of figure 6 with $d = -5 \times 10^{-6}$ (left) and $d = -10^{-6}$ (right). We plot the evolution for the mode corresponding to the peak in the power spectrum and we denote the horizon crossing with a small blue circle. The red and green shaded regions have the same meaning as in figure 5.

However, in that example, we must go slightly off the attractor regime, and compensate for the decrease of n_s by an increase of n_s due to the uplift by $V_{\rm up} = M^2 \chi_0^2 / 4$ [35]).

Things are different for polynomial hybrid attractors that we introduce in the next section, where one does not need to rely on uplifting for consistency with the Planck data. But for the exponential attractors discussed in this section, the proximity of the attractor regime is also very helpful. For example, if $\Delta N = 10$ and $N_* \sim 55$, the attractor prediction ignoring the uplifting would be $n_s \sim 0.956$. This would inform us that with an account taken of uplifting the value of n_s does not go below 0.956, and we only need an uplift increasing n_s by less than 0.01 to make it consistent with the Planck results. It is always possible to do it; in the large uplift limit one can bring n_s all the way up to $n_s = 1$ [35]. This healing power of uplift may play a significant role in the development of advanced inflationary models compatible with the changing observational landscape, where the attempts to resolve the H_0 problem may push us towards considering inflationary models with large n_s [84–87].

Growth of perturbations. Before concluding, we note that since the perturbations in our model grow very large, care should be taken for them not to backreact on the background evolution. As a naive criterium, which should anyway give a good estimate of when backreaction is negligible, we compare the background values of φ and χ to the evolution of the corresponding perturbations $\sim \sqrt{\mathcal{P}_{Q_\varphi}}$ and $\sim \sqrt{\mathcal{P}_{Q_\chi}}$. Here, we denote the gauge-invariant perturbations to the two fields by Q_φ and Q_χ. We show this in figure 9, where we plot the evolution of the $k_{\rm peak}$ modes, which is the one that takes larger values.

In the left panel, corresponding to the baseline case, where $\mathcal{P}_{\mathcal{R}}(k_{\rm peak}) \sim 0.007$, we see that the perturbations are always subdominant with respect to the background fields. In particular, after the perturbation to χ crosses the horizon, where it takes the typical value $H/2\pi$, it starts growing because of the tachyonic instability, but we see that the background value for χ is always at least ~ 15 times larger. We therefore conclude that in this case the perturbations should not affect the background evolution and our results are robust. As another example, we show the evolution for $k_{\rm peak}$ in the case of a smaller $d = -10^{-6}$, also
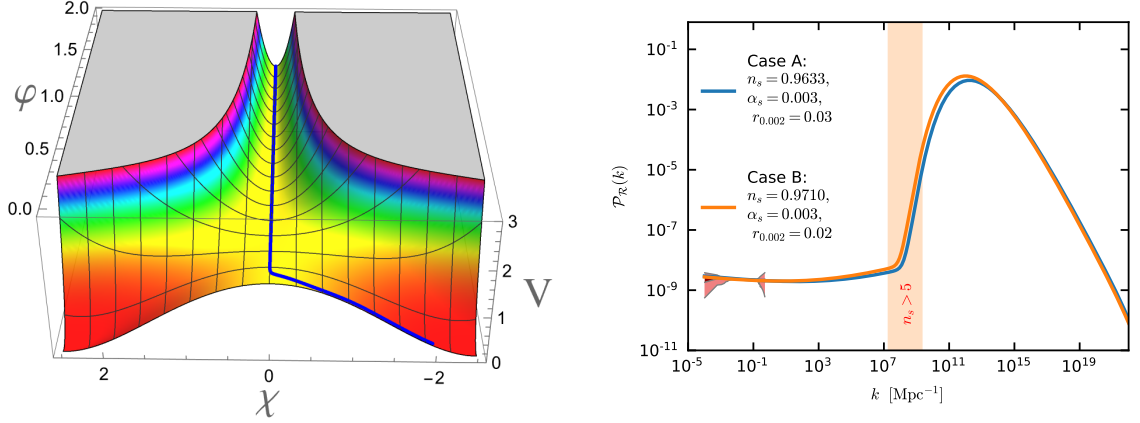
Figure 10. Examples with a larger n_s. We use the following parameters. Case A: $\alpha = 0.9$, $\tilde{m} = 0.35$, $\chi_0 = 2.5$, $\tilde{g} = 3.7$, $d = 5 \times 10^{-6}$. Case B: $\alpha = 0.6$, $\tilde{m} = 0.35$, $\chi_0 = 2.5$, $\tilde{g} = 5$, $d = 5 \times 10^{-6}$. The parameter M is fixed to match the COBE normalization and φ_i to achieve 70 e-folds of inflation. The potential is shown in units M^2. The trajectory in the left panel is shown for Case A, but is representative also of Case B, which shares the same features.

shown in figure 6. We see that also in this case perturbations remain small compared to the background value, although now $\sqrt{\mathcal{P}_{Q_\chi}}$ is only a factor of ~ 3 smaller, so the two quantities are of the same order of magnitude. However, this case has a very large peak amplitude $\mathcal{P}_\mathcal{R}(k_{\mathrm{peak}}) \sim 0.17$ so that it is excluded by the over-production of PBHs and also by current Pulsar Timing Array (PTA) limits on the SGWB induced by the scalar perturbations at second order (see next section).

A larger n_s. Although the example above is perfectly consistent with CMB observations, it is interesting to explore whether larger values of n_s can be attained in our model. We show two examples in figure 10, where n_s falls both on the right of the sweet spot of the Planck/BICEP/Keck Array. Note that also a non-negligible amount of running is produced, which is nevertheless consistent with the constraints from Planck [41]. As seen in the left panel, the main difference with respect to the baseline evolution is that, since g is larger and φ_c smaller, the hybrid field χ starts to move later during inflation, with a resulting shorter waterfall stage. The CMB scales therefore test the region where the plateau is flatter and n_s bluer. However, also in this case, the uplifting potential is quite large, i.e. the ratio V_0/V_{up} is small, and we cannot rely on the simple attractor relation $n_s = 1 - 2/(N_* - \Delta N)$, as discussed above.

We also note another interesting feature of the power spectrum in figure 10. The power spectra in the yellow-shaded region rises with a spectral index of roughly 10.9 and 11.2 for Case A and B respectively. This growth is much steeper than $n_s \sim 5$ (plus a weak running) which is the limit in the case of canonical single field inflation [94, 95], confirming that multiple field effects can easily overcome such limit [6, 7, 9].

6 Stochastic gravitational wave background generated at horizon re-entry

It is well known that scalar and tensor perturbations are decoupled at linear order. However, they are mixed at higher orders in perturbation theory. In particular, scalar perturbations act as a source of gravitational waves at second order in perturbation theory when they

re-enter the Hubble radius during the radiation dominated era[7] [37–39]. If their amplitude is large enough, the resulting SGWB can fall into the sensitivity of future gravitational wave interferometers, that can therefore be used to test the physics of Hybrid inflation. It is therefore crucial to make accurate predictions on the spectral shape of the SGWB.

The energy density of the SGWB at present time is given by [101, 102]:

$$
\Omega_{\text{ind}}(k) = 0.387 \, \Omega_{\text{R}} \left(\frac{g_{*,s}^4 g_*^{-3}}{106.75} \right)^{-\frac{1}{3}} \frac{1}{6} \int_{-1}^{1} \mathrm{d}x \int_{1}^{\infty} \mathrm{d}y \, \mathcal{P}_{\mathcal{R}} \left(\frac{y-x}{2} k \right) \mathcal{P}_{\mathcal{R}} \left(\frac{x+y}{2} k \right) F(x,y) \,,
$$
(6.1)

where $\Omega_{\text{R}} = 5.38 \times 10^{-5}$ is the radiation abundance [103], the effective numbers of degrees of freedom, $g_{*,s}$ and g_*, are evaluated at the moment when the constant abundance is reached, roughly coinciding with the horizon crossing time, and

$$
F(x,y) = \frac{288(x^2 + y^2 - 6)^2(x^2 - 1)^2(y^2 - 1)^2}{(x-y)^8(x+y)^8}
$$
$$
\times \left[\left(x^2 - y^2 + \frac{x^2 + y^2 - 6}{2} \log \left| \frac{y^2 - 3}{x^2 - 3} \right| \right)^2 + \frac{\pi^2}{4}(x^2 + y^2 - 6)^2 \theta(y - \sqrt{3}) \right]. \quad (6.2)
$$

We show in figure 11 the SGWB spectra corresponding to the scalar power spectra shown in figure 6, compared to the sensitivity of future experiments. We also plot in cyan the recent claim of a detection from the NANOGrav collaboration [104]. However, since there is no evidence for the so-called Hellings and Downs curve, which would be the smoking gun for a gravitational wave background detection, we interpret the data point as an upper limit (see [105] for a recent study on the implications on peaked power spectra from inflation).

We note that Ω_{GW} depends on the model parameters qualitatively in the same way as the curvature power spectrum. This is obvious because the integral in eq. (6.1) suggests that $\Omega_{\text{GW}}(f) \propto \mathcal{P}_{\mathcal{R}}^2(f)$. We see that the background produced in Hybrid inflationary model typically falls in the sensitivity region of PTA experiments (magenta shaded area) and space-based gravitational waves interferometers such as LISA (turquoise-green shaded area) and more futuristic ones like BBO and DECIGO (grey shaded area). Some values of the parameter space, in particular those featuring a too-large amplification of the spectrum are already excluded by current PTA limits from the NANOGrav collaboration. Interestingly, the models excluded are those for which our analysis is less reliable and we should start to take into account stochastic effects the backreaction on the background dynamics during inflation, see a discussion in section 4, and in the discussion of figure 9.

Reconstructing the spectral shape of the SGWB is a target of future gravitational wave experiments [106, 107], it is thus important to provide simple templates for $\Omega_{\text{GW}}(f)$ that can be readily used in such searches. Since the computation of the primordial curvature power spectrum, and therefore of the induced SGWB, has to be performed numerically, such template is intended to be purely phenomenological and a one-to-one connection with the model parameters is not straightforward. Nevertheless, having a template that closely matches the exact result has the clear advantage of simplicity. In case of a detection of the

---

[7]In principle, since the perturbations produced during inflation are quite large, in addition to the gravitational waves produced during the radiation era, we could also expect a sizable background to be sourced already during inflation [96]. However, as shown in ref. [97], its amplitude is suppressed, relative to that produced after inflation, by powers of ϵ and $\eta_\perp/H$. Since both factors are much smaller than 1 in our model, we ignore this contribution.
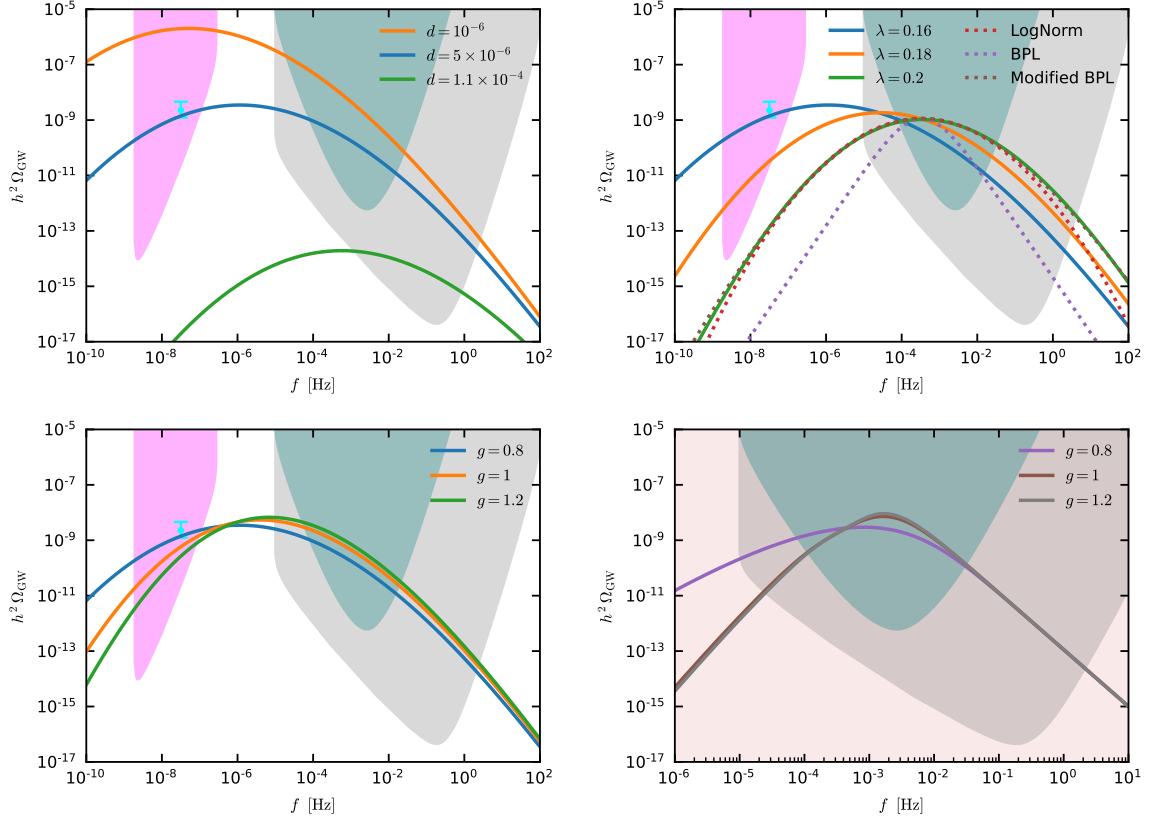
Figure 11. SGWB sourced by the large amplitude perturbations. We consider the same parameters as in figure 6. Magenta, turquoise-green and grey shaded regions correspond to the sensitivities of SKA [98], LISA [99] and BBO/DECIGO [100].

phenomenological template, the exact signal can be compared numerically and constraints on the true model parameters can be set.

Focusing for simplicity on LISA, we see that, depending on where the peak is located, we may need a more complex template to capture the signal. For example, if the peak falls outside the sensitivity, the SGWB can be just described by a simple power law, as for the blue line in the top-left panel of figure 11. If, on the other hand, the peak is exactly in the sensitivity range of LISA, a simple power-law would not be precise enough to describe the richer structure of $\Omega_{\rm GW}(f)$ and some more advanced functions to describe the peak will be needed. This is the case of the green line in the top-right panel of figure 11.

As we can see, a simple lognormal shape for $\Omega_{\rm GW}$, i.e. a Gaussian in log-space, captures very well the region close to the peak, but it fails to describe the power-law behaviors at frequencies smaller and larger than the peak frequency $f_{\rm peak}$. While this accuracy is probably acceptable for LISA, whose sensitivity band is narrow enough not to see this deviation, it would be nice to have an even more accurate template, suitable for the next-generation of space based experiments. Also, this template is important to describe situations, such as the green line in the bottom-left panel of figure 11, where the background falls in the sensitivity range of multiple experiments.

We see that a simple broken power law is not able to reproduce our signal either. A solution is to smooth the transition between the two power-laws at the pivot frequency $f_{\rm peak}$

and adopt the following smoothed broken power-law template:

$$h^2\Omega_{\mathrm{GW}}(f) = A\,\frac{\mathcal{F}(f,\,f_{\mathrm{peak}},\,n_1,\,n_2,\,\Delta)}{\mathcal{F}(f_{\mathrm{peak}},\,f_{\mathrm{peak}},\,n_1,\,n_2,\,\Delta)}\,, \tag{6.3}$$

where

$$\mathcal{F}(f,\,f_{\mathrm{peak}},\,n_1,\,n_2,\,\Delta) = \frac{\left[\frac{f}{f_{\mathrm{peak}}}\left(-\frac{n_1}{n_2}\right)^{\Delta}\right]^{n_1}}{\left\{\frac{1}{2}\left[1+\left(\frac{f}{f_{\mathrm{peak}}}\left(-\frac{n_1}{n_2}\right)^{\Delta}\right)^{1/\Delta}\right]\right\}^{\Delta(n_1-n_2)}}\,. \tag{6.4}$$

As can be seen, with a proper choice of parameters, the template accurately matches the exact result and can therefore used in phenomenological searches for the SGWB produced in our model and similar ones. Indeed, we note that the GW signal produced by our model is also common to other realizations of hybrid inflation, that however produce different predictions at large scales, as previously discussed. The synergy of large and small scale data would be instrumental in pinning down the fundamental embedding of the hybrid inflation mechanism.

7 Hybrid polynomial attractors

The hybrid attractor scenario described in this paper was mainly devoted to the so-called exponential attractors, such as $V_0\tanh^2\left(\frac{\varphi}{\sqrt{6\alpha}}\right)$, where the potential of the field φ approaches the plateau exponentially,

$$V(\varphi) = V_0\left(1 - e^{-\varphi/\mu} + \ldots\right)\,. \tag{7.1}$$

But there is yet another broad class of cosmological attractors, where the potential approaches the plateau more slowly, not exponentially but as inverse powers of the inflaton field,

$$V \sim V_0\left(1 - \frac{\mu^k}{\varphi^k} + \ldots\right)\,, \tag{7.2}$$

where k can be any (integer or not) positive constant. The simplest examples of such potentials are given by

$$V = V_0\,\frac{\varphi^k}{\varphi^k + \alpha^k}\,. \tag{7.3}$$

They were called polynomial attractors [54]. Such potentials may appear in several different contexts, such as KKLTI inflation [108], pole inflation [109], and also as a special version of α-attractors [54].

In all of these cases, at $\alpha \ll 1$ in the large N limit these potentials have universal attractor predictions, independently of other details of the potential indicated by the ellipsis ... in eq. (7.2). In particular, the spectral index n_s depends only on k [110]:

$$n_s = 1 - \frac{2}{N}\frac{k+1}{k+2}\,. \tag{7.4}$$

Here we will consider the hybrid inflation scenario where instead of the potential $\frac{m^2}{2}\phi^2$ we will use a potential $V = \frac{m^2}{2}\frac{\alpha^2\varphi^2}{\varphi^2+\alpha^2}$. At $\varphi^2 \ll \alpha^2$ this potential is given by the familiar expression $\frac{m^2}{2}\varphi^2$, but at $\varphi^2 \gg \alpha^2$ it approaches a plateau $V_0 = \frac{m^2\alpha^2}{2}$.
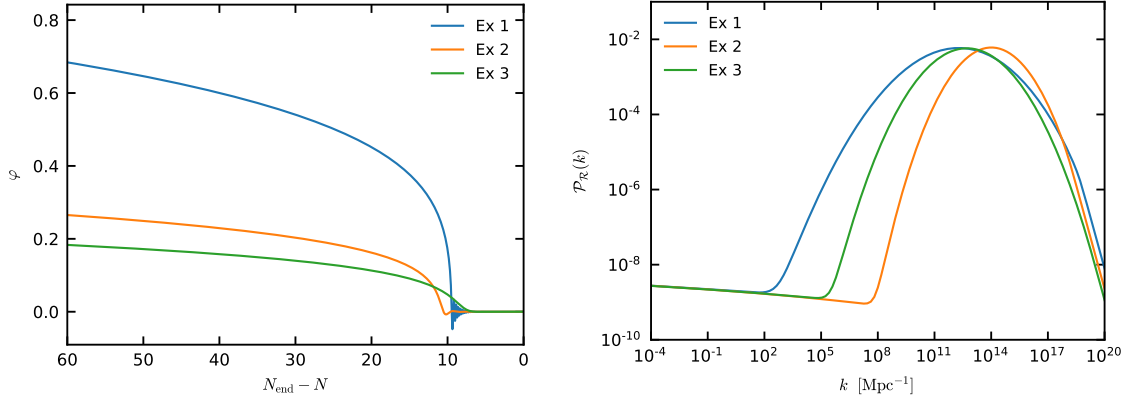
Figure 12. [Left] Evolution of the field φ in the hybrid polynomial attractors model. [Right] Primordial power spectra. The parameters for each example are reported in table 1.

	d	$\tilde{m}\alpha$	$\tilde{g}$	ΔN	$n_{s,\text{KKLTI}}$	$n_{s,\text{num}}$
Example 1	-2×10^{-7}	0.7	2	9.43	0.9671	0.9670
Example 2	-10^{-7}	0.3	6	11.00	0.9659	0.9652
Example 3	-6×10^{-8}	0.05	8	8.91	0.9674	0.9662

Table 1. Parameter combination used in our examples, and corresponding values for ΔN and the scalar spectral index.

Ignoring, for simplicity, the hybrid inflation uplifting, these models have universal predictions [110]

$$n_{s,\text{KKLTI}} = 1 - \frac{3}{2N}\,, \qquad r = \frac{\sqrt{2}\alpha}{N^{3/2}}\,. \tag{7.5}$$

The corresponding hybrid inflation potential based on this particular version of the polynomial attractor is given by

$$V_{\text{poly}}(\chi, \varphi) = M^2 \left[\frac{(\chi^2 - \chi_0^2)^2}{4\chi_0^2} + \frac{\tilde{m}^2}{2} \frac{\alpha^2 \varphi^2}{\varphi^2 + \alpha^2} + \frac{\tilde{g}^2}{2} \varphi^2 \chi^2 + d\chi \right]. \tag{7.6}$$

In figure 12, we provide some examples of the evolution of the field φ in this model, together with the associated power spectra. We fix the following parameters $\alpha = 0.05$, $\lambda = 1/\chi_0^2 = 0.3$ and M is chosen to match the COBE normalization, as usual. The small value of α is chosen here to take advantage of the attractor regime of polynomial attractors [109]. The other parameters are varied according the following table. As discussed in the previous section, the number of e-folds that is used in eq. (7.5) is $N_{\text{KKLTI}} = N_* - \Delta N = 55 - \Delta N$, where we assume $N_* = 55$.

We can see that the main features of the peak in the power spectrum are essentially the same as in the exponential hybrid attractor models. The main difference is that the predictions at large scales follow a different attractor. Like in the previous section, we observe that increasing $\tilde{m}\alpha$ brings the analytical predictions into closer agreement with the numerical results for n_s. However, unlike in the case of exponential attractors, here this allows us to take full advantage of the attractor nature of the model. Indeed, since now $n_s = 1 - 3/2(N_* - \Delta N)$, the attractor predictions are consistent with Planck data even for the value of $\Delta N \sim 10$

needed to get a phenomenologically interesting peak at small scales in this model. Therefore in this context we do not need to rely on uplifting to shift the attractor prediction upwards to larger values of n_s. However, we can use this mechanism if we want to consider models with larger values of ΔN, or if we want to increase n_s even further.

8   Discussion

Models of inflation producing a large amplitude peak at small scales are the subject of a very active field of research, primarily because they potentially lead to the production of PBHs and a SGWB testable with future gravitational wave facilities. Historically, hybrid inflation [2, 3] was one of the first models where such an amplification of power was considered [1], see also [111–118]. In this paper, we investigated the possibility to generate perturbations with a very high peak in the spectrum in its recently developed α-attractor generalization [35] of the hybrid inflation scenario and discussed its consequences for PBH and SGWB production.

This scenario describes an inflaton field φ interacting with a Higgs-type field χ in such a way that the latter becomes tachyonic when φ becomes smaller than some critical value φ_c. In the simplest cases, the absolute value of the tachyonic mass of the field χ becomes much greater than the Hubble constant H at $\varphi < \varphi_c$. Is such cases, the field χ falls down to the minimum of the potential at $\chi = \chi_0$ and inflation abruptly ends at $\varphi \approx \varphi_c$ [2, 3].

However, for $\chi_0 \gg 1$ the tachyonic mass of the field χ at $\varphi \lesssim \varphi_c$ remains much smaller than H. In such cases, inflation continues while the field χ slowly rolls down towards the minimum of $V(\chi)$. As we explained in this paper, in this case, at $\varphi < \varphi_c$, the universe enters the eternal inflation regime: in some parts of the universe inflation eternally continues at $\chi = 0$, whereas in many other parts inflation ends within a relatively small number of e-foldings ΔN. This leads to enormous perturbations of density on the scale proportional to $e^{\Delta N}$, which results in copious production of PBHs and eternally inflating parts of the universe, including eternally inflating topological defects.

This is a very general property of this class of models, which does not require any fine-tuning, so it is very easy to produce a very high peak of perturbations and PBH in this scenario. The only problem is how to keep the situation under control, to avoid overproduction of both PBHs and eternally inflating topological defects inside the observable part of the universe.

One way to do it is to reduce χ_0, which stops eternal inflation and suppresses the amplitude of perturbations [1, 44]. However, this is not sufficient to solve the problem of supermassive topological defects. Another problem is how to make a large bump at some intermediate range of e-foldings and simultaneously have perturbation with $n_s \sim 0.96$–0.97 compatible with the Planck data.

In this paper, we showed that it is possible to solve all of these problems in the α-attractor generalization of hybrid inflation [35] if we add a tiny linear term $\mu^3 \chi$ to the potential. This term pushes the inflationary trajectory slightly off the ridge of the potential. This solves the problem of topological defects and simultaneously decreases the amplitude of the perturbation in a controllable way. The position and the width of the peak can be controlled by other parameters of the hybrid inflation potential.

Phenomenologically, key features of this model are the agreement with CMB measurements from Planck and the production of PBHs and SGWB at smaller scales, that offer nice prospects for testing it in the future. Indeed, many realizations of hybrid inflation were excluded by the earliest Planck release [45]. Thanks to the α-attractor modification of the model, one can find a broad range of parameters where n_s and r are consistent with the

latest Planck/BICEP/Keck Array results. On smaller scales, the model is flexible enough to produce bumps at different locations and with different shapes, making it possible to produce very light to heavy PBHs, possibly constituting the totality of the Cold Dark Matter in our universe if the peak is located at the right position. While the formation of PBHs is mainly sensitive to the overall amplitude of the peak, future observations of the induced SGWB have the potential to unveil its spectral shape over orders of magnitude in frequency. Our model thus constitute a primary target of future searches for stochastic backgrounds of gravitational waves. To this purpose, we have also derived a very simple template that perfectly captures the frequency profile of the gravitational wave energy spectrum, and can be readily used by the gravitational wave community to test our model. We stress that the GW signal described by our template, first proposed in our paper, is quite generic to the hybrid inflation mechanism. However, the embedding of hybrid inflation into the α-attractor framework leads to predictions at large scales that are consistent with current data, making the synergy of GW experiments with large scale structure measurements crucial to identify the origin of the hybrid inflation mechanism.

We note that the hybrid attractor model proposed in [35], and further developed in this paper, represents a simple generalization of the basic hybrid inflation model [2, 3]. In the appendix A it is shown how this scenario can be implemented in supergravity. One can also generalize this two-field model to include many other fields. In particular, instead of the inflaton potential $\frac{m^2}{2}\varphi^2$ one can consider O(2) invariant potential $\frac{m^2}{2}(\varphi_1^2 + \varphi_2^2)$. In such model instead of domain walls we would have global strings. If we consider a potential $\frac{m^2}{2}(\varphi_1^2 + \varphi_2^2 + \varphi_3^2)$ we would have global monopoles. By considering more general potentials for the field χ, including hilltop inflationary potentials such as $(\chi^4 - \chi_0^4)^2$, or the Coleman-Weinberg potential used in new inflation, one may have a second inflationary stage with an extremely small value of χ_0. In such models one may find a different way to control the amplitude of the spectrum and avoid problems with topological defects. In fact, as shown in [119, 120], in certain cases such defects may independently contribute to the PBH production.

Acknowledgments

A Supergravity implementation of hybrid attractors

A.1 Hybrid α-attractors with a canonical waterfall field, adding axions

In the context of the PBH production hybrid inflation was studied in supersymmetric F- and D-term inflation [44]. All fields in these models have canonical kinetic terms, therefore the choice of parameters consistent with CMB as well as leading to PBH production is not easy to make. For example in D-term supergravity model the Planck-like FI term and a superpotential with large coupling are required.

Our models have plateau potentials with non-canonical geometric inflaton at the first stage of inflation, which facilitates their agreement with the CMB data.

The α-attractor versions of hybrid inflation models were proposed and studied in [35]. The first stage of inflation was defined by a plateau potential for the field φ originating from a geometric hyperbolic disk geometry with the Kähler curvature $\mathcal{R} = -\frac{2}{3\alpha}$. The waterfall phase of hybrid inflation is due to a second field χ which was also defined in [35] by a geometric hyperbolic disk geometry with the Kähler curvature $\mathcal{R} = -\frac{2}{3\beta}$.

In the models we study here we take the waterfall χ to be a canonical field, $\beta \to \infty$. For our purpose to study high peaks in inflationary perturbations any value of $\beta > 1$ is suitable, not much depends on it. Small values of β are more interesting if we design the second stage of inflation as a quintessence cosmology, which is not the purpose of this paper. Therefore, in our case a canonical waterfall field is the simplest possibility.

Here we will present the supergravity version of the cosmological models for a geometric inflaton φ and a canonical waterfall field χ studied in this paper. These models can also be obtained from supergravity versions of general hybrid inflation in [35] in the limit $\beta \to \infty$.

We start as follows

$$\frac{\mathcal{L}}{\sqrt{-g}} = \frac{R}{2} - \frac{(\partial_\mu \phi)^2}{2\left(1 - \frac{\phi^2}{6\alpha}\right)^2} - \frac{(\partial_\mu \chi)^2}{2} - V(\chi, \phi), \tag{A.1}$$

where

$$V(\phi, \chi) = M^2 \Big(V_{\text{hybrid}}(\chi, \phi) + V_{\text{lin}}(\chi) \Big). \tag{A.2}$$

Here

$$V_{\text{hybrid}}(\phi, \chi) = \frac{m^2}{2} \phi^2 + \frac{g^2}{2} \phi^2 \chi^2 + \frac{(\chi^2 - \chi_0^2)^2}{4\chi_0^2}, \tag{A.3}$$

$$V_{\text{lin}}(\chi) = d\chi. \tag{A.4}$$

To be careful, one should also subtract a tiny constant $\approx d\,\chi_0$ to ensure smallness of the cosmological constant at the minimum, but this term can be ignored in the investigation of inflation.

Upon transformation to canonical variables $\phi = \sqrt{6\alpha}\,\tanh\frac{\varphi}{\sqrt{6\alpha}}$ we find

$$\frac{\mathcal{L}}{\sqrt{-g}} = \frac{R}{2} - \frac{1}{2}(\partial_\mu \varphi)^2 - \frac{1}{2}(\partial_\mu \chi)^2 - V(\varphi, \chi). \tag{A.5}$$

The hybrid potential (A.2) as a function of φ and χ becomes (2.3)

$$V(\varphi, \chi) = M^2 \left[3\alpha \tanh^2 \frac{\varphi}{\sqrt{6\alpha}} (\tilde{m}^2 + \tilde{g}^2 \chi^2) + \frac{(\chi^2 - \chi_0^2)^2}{4\chi_0^2} + d\chi \right]. \tag{A.6}$$

The model given in eqs. (A.5), (A.6) is a model with 2 bosonic fields. In the main part of the paper we studied the cosmological properties of this model.

We would like to embed this bosonic model into a supergravity model. Such an embedding is not unique, we choose here a relatively simple one. The first step is to relate each of the scalars φ and χ to complex scalars Z_1, Z_2. This means also that two scalars of the original bosonic models are supplemented by two axions.

$$Z_1 = ze^{i\theta_1} = \tanh \frac{\varphi}{\sqrt{6\alpha}} e^{i\theta_1}, \qquad Z_2 = \frac{1}{\sqrt{2}} \chi e^{i\theta_2}. \tag{A.7}$$

Now we need to make sure that there is a minimum in θ_i directions at $\theta_i = 0$, so that both axions are stabilized at their vanishing value.

Many cosmological supergravity models associated with string theory and uplifting anti-D3 branes which were proposed and studied during the last few years involve an additional nilpotent chiral superfield X such that $X^2 = 0$. It represents non-linearly realized supersymmetry of the Volkov-Akulov type.

The reason why the embedding proposed in (A.7) is relatively simple is the fact, established earlier in [121–123], that there is a universal geometric mechanism of stabilization of the inflaton partner during inflation (or in general, of the imaginary part of the complex scalar), based on the bisectional curvature. In our case, this is a statement that the fields $\text{Im}\, Z_i$ can be stabilized at $\text{Im}\, Z_i = 0$, i.e. at $\theta_1 = \theta_2 = 0$, which reduces our supergravity model to the bosonic cosmological model we study in this paper. In presence of the nilpotent superfield one can add to the Kähler potential a bisectional curvature term of the form

$$K_{\text{bisec}} = X\bar{X}A(Z,\bar{Z})\text{Im}^2 Z \tag{A.8}$$

for each of the axions $\text{Im}\, Z$ which we want to stabilize. These terms with appropriate choice of the function $A(Z,\bar{Z})$ add a positive mass terms to each of the axions at all positions in inflationary trajectory.

In fact, very often our earlier models in [123] were stabilized at the vanishing values of the axions even without the need for bisectional curvature terms. This feature is provided by special properties of these models which we also used in [124] and will use here.

A.2 Supergravity model with stabilized axions

There are 3 chiral superfields, Z_1, Z_2 and a nilpotent one X. The Kähler potential and the superpotential are:

$$K = K_{X\bar{X}}X\bar{X} - 3\alpha \log\left(1 - Z_1\overline{Z_1}\right) + Z_2\overline{Z_2}, \quad K_{X\bar{X}} = \frac{F_X^2}{F_X^2 + \mathcal{V}\left(Z_1, \overline{Z_1}, Z_2, \overline{Z_2}\right)}, \tag{A.9}$$

$$W = M(F_X X + W_0)\left(1 - Z_1^2\right)^{\frac{3\alpha}{2}} e^{-\frac{Z_2^2}{2}}. \tag{A.10}$$

Here $\mathcal{V}\left(Z_1, \overline{Z_1}, Z_2, \overline{Z_2}\right)$ is an arbitrary function. To match the potential of the hybrid α-attractors (A.6) we will take

$$\mathcal{V} = M^2\left\{3\alpha Z_1\overline{Z_1}\left(\tilde{m}^2 + \tilde{g}^2 Z_2\overline{Z_2}\right) + \frac{1}{4\chi_0^2}\left[\left(\frac{Z_2 + \overline{Z_2}}{\sqrt{2}}\right)^2 - \chi_0^2\right]^2 + d\frac{Z_2 + \overline{Z_2}}{\sqrt{2}}\right\}. \tag{A.11}$$

The total potential

$$V^{\text{super}} = e^K(|DW|^2 - 3|W|^2) \tag{A.12}$$

as a function of complex fields Z_1, Z_2 at $X = 0$ is complicated, but at real Z_1, Z_2 it is reduced to (A.6) where in addition there is a cosmological constant term $\Lambda = F_X^2 - 3W^2$

$$V^{\text{super}}|_{Z_i = \overline{Z}_i, X=0} = \Lambda + V(\varphi, \chi). \tag{A.13}$$

Using Kähler invariance of the potential (A.12) we can present an alternative form of K and W which helps to explain the reason why the axions are easy to stabilize in this class of

models. The first term in K is the same as in (A.9) but the second and the third, as well as W are different due to a Kähler transformation preserving the potential

$$K = K_{X\bar{X}}X\bar{X} - \frac{3\alpha}{2}\log\frac{\left(1 - Z_1\overline{Z_1}\right)}{(1 - Z_1^2)(1 - \overline{Z_1}^2)} - \frac{1}{2}(Z_2 - \overline{Z_2})^2 \,, \tag{A.14}$$

$$W = M\left(F_X X + W_0\right). \tag{A.15}$$

The Kähler potential $-\frac{3\alpha}{2}\log\frac{\left(1 - Z_1\overline{Z_1}\right)}{(1 - Z_1^2)(1 - \overline{Z_1}^2)} - \frac{1}{2}(Z_2 - \overline{Z_2})^2$ vanishes at $Z_i = \overline{Z}_i$ by design, and it has terms proportional to axions $-(Z_i - \overline{Z}_i)^2$. The shift symmetry for axions $Z \to Z + ic$ is therefore broken already by K and in most cases axions are stabilized even without additional terms with bisectional curvature (A.8), as shown in [123].

It was also important here that one can make a choice of the function $\mathcal{V}\left(Z_1, \overline{Z_1}, Z_2, \overline{Z_2}\right)$ in eq. (A.9) in the Kähler potential of the nilpotent field $K_{X\bar{X}}$ supporting the stabilization of the axions initiated by the choice of the Kähler potential of the chiral superfields Z_i.

In particular, for the parameters used in this paper for the model in (A.6) we have checked that axions are stabilized at $Z_i = \overline{Z}_i$ and they have large positive masses even without bisectional curvature terms (A.8). For more general parameters, in any case the bisectional curvature terms (A.8) can always be added and therefore we have promoted our bosonic models to supergravity models consistently.

References

[1] J. Garcia-Bellido, A.D. Linde and D. Wands, *Density perturbations and black hole formation in hybrid inflation*, *Phys. Rev. D* **54** (1996) 6040 [astro-ph/9605094] [INSPIRE].

[2] A.D. Linde, *Axions in inflationary cosmology*, *Phys. Lett. B* **259** (1991) 38 [INSPIRE].

[3] A.D. Linde, *Hybrid inflation*, *Phys. Rev. D* **49** (1994) 748 [astro-ph/9307002] [INSPIRE].

[4] A. Dolgov and J. Silk, *Baryon isocurvature fluctuations at small scales and baryonic dark matter*, *Phys. Rev. D* **47** (1993) 4244 [INSPIRE].

[5] A.R. Brown, *Hyperbolic Inflation*, *Phys. Rev. Lett.* **121** (2018) 251601 [arXiv:1705.03023] [INSPIRE].

[6] J. Fumagalli, S. Renaux-Petel, J.W. Ronayne and L.T. Witkowski, *Turning in the landscape: a new mechanism for generating Primordial Black Holes*, arXiv:2004.08369 [INSPIRE].

[7] G.A. Palma, S. Sypsas and C. Zenteno, *Seeding primordial black holes in multifield inflation*, *Phys. Rev. Lett.* **125** (2020) 121301 [arXiv:2004.06106] [INSPIRE].

[8] M. Braglia et al., *Generating PBHs and small-scale GWs in two-field models of inflation*, *JCAP* **08** (2020) 001 [arXiv:2005.02895] [INSPIRE].

[9] M. Braglia, X. Chen and D.K. Hazra, *Probing Primordial Features with the Stochastic Gravitational Wave Background*, *JCAP* **03** (2021) 005 [arXiv:2012.05821] [INSPIRE].

[10] L. Iacconi, H. Assadullahi, M. Fasiello and D. Wands, *Revisiting small-scale fluctuations in α-attractor models of inflation*, *JCAP* **06** (2022) 007 [arXiv:2112.05092] [INSPIRE].

[11] R. Kallosh and A. Linde, *Dilaton-axion inflation with PBHs and GWs*, *JCAP* **08** (2022) 037 [arXiv:2203.10437] [INSPIRE].

[12] P. Ivanov, P. Naselsky and I. Novikov, *Inflation and primordial black holes as dark matter*, *Phys. Rev. D* **50** (1994) 7173 [INSPIRE].

[13] J. Garcia-Bellido and E. Ruiz Morales, *Primordial black holes from single field models of inflation*, *Phys. Dark Univ.* **18** (2017) 47 [arXiv:1702.03901] [INSPIRE].

[14] H. Motohashi and W. Hu, *Primordial Black Holes and Slow-Roll Violation*, *Phys. Rev. D* **96** (2017) 063503 [arXiv:1706.06784] [INSPIRE].

[15] C. Germani and T. Prokopec, *On primordial black holes from an inflection point*, *Phys. Dark Univ.* **18** (2017) 6 [arXiv:1706.04226] [INSPIRE].

[16] G. Ballesteros and M. Taoso, *Primordial black hole dark matter from single field inflation*, *Phys. Rev. D* **97** (2018) 023501 [arXiv:1709.05565] [INSPIRE].

[17] I. Dalianis, A. Kehagias and G. Tringas, *Primordial black holes from α-attractors*, *JCAP* **01** (2019) 037 [arXiv:1805.09483] [INSPIRE].

[18] S.V. Ketov, *Multi-Field versus Single-Field in the Supergravity Models of Inflation and Primordial Black Holes*, *Universe* **7** (2021) 115 [INSPIRE].

[19] Y.-F. Cai et al., *One small step for an inflaton, one giant leap for inflation: A novel non-Gaussian tail and primordial black holes*, *Phys. Lett. B* **834** (2022) 137461 [arXiv:2112.13836] [INSPIRE].

[20] S. Balaji, J. Silk and Y.-P. Wu, *Induced gravitational waves from the cosmic coincidence*, *JCAP* **06** (2022) 008 [arXiv:2202.00700] [INSPIRE].

[21] S.R. Geller, W. Qin, E. McDonough and D.I. Kaiser, *Primordial black holes from multifield inflation with nonminimal couplings*, *Phys. Rev. D* **106** (2022) 063535 [arXiv:2205.04471] [INSPIRE].

[22] S. Pi and J. Wang, *Primordial Black Hole Formation in Starobinsky's Linear Potential Model*, arXiv:2209.14183 [IPMU22-0047] [INSPIRE].

[23] S. Pi, Y.-L. Zhang, Q.-G. Huang and M. Sasaki, *Scalaron from R^2-gravity as a heavy field*, *JCAP* **05** (2018) 042 [arXiv:1712.09896] [INSPIRE].

[24] A. Ashoorioon, A. Rostami and J.T. Firouzjaee, *EFT compatible PBHs: effective spawning of the seeds for primordial black holes during inflation*, *JHEP* **07** (2021) 087 [arXiv:1912.13326] [INSPIRE].

[25] K. Inomata, E. McDonough and W. Hu, *Primordial black holes arise when the inflaton falls*, *Phys. Rev. D* **104** (2021) 123553 [arXiv:2104.03972] [INSPIRE].

[26] K. Inomata, E. McDonough and W. Hu, *Amplification of primordial perturbations from the rise or fall of the inflaton*, *JCAP* **02** (2022) 031 [arXiv:2110.14641] [INSPIRE].

[27] I. Dalianis and G.P. Kodaxis, *Reheating in Runaway Inflation Models via the Evaporation of Mini Primordial Black Holes*, *Galaxies* **10** (2022) 31 [arXiv:2112.15576] [INSPIRE].

[28] K. Boutivas, I. Dalianis, G.P. Kodaxis and N. Tetradis, *The effect of multiple features on the power spectrum in two-field inflation*, *JCAP* **08** (2022) 021 [arXiv:2203.15605] [INSPIRE].

[29] K. Inomata, M. Braglia and X. Chen, *Questions on calculation of primordial power spectrum with large spikes: the resonance model case*, *JCAP* **04** (2023) 011 [arXiv:2211.02586] [INSPIRE].

[30] J. Garriga, A. Vilenkin and J. Zhang, *Black holes and the multiverse*, *JCAP* **02** (2016) 064 [arXiv:1512.01819] [INSPIRE].

[31] H. Deng, J. Garriga and A. Vilenkin, *Primordial black hole and wormhole formation by domain walls*, *JCAP* **04** (2017) 050 [arXiv:1612.03753] [INSPIRE].

[32] M.Y. Khlopov, *Primordial Black Holes*, *Res. Astron. Astrophys.* **10** (2010) 495 [arXiv:0801.0116] [INSPIRE].

[33] B. Carr, K. Kohri, Y. Sendouda and J. Yokoyama, *Constraints on primordial black holes*, *Rept. Prog. Phys.* **84** (2021) 116902 [`arXiv:2002.12778`] [ɪɴSPIRE].

[34] B. Carr and F. Kuhnel, *Primordial black holes as dark matter candidates*, *SciPost Phys. Lect. Notes* **48** (2022) 1 [`arXiv:2110.02821`] [ɪɴSPIRE].

[35] R. Kallosh and A. Linde, *Hybrid cosmological attractors*, *Phys. Rev. D* **106** (2022) 023522 [`arXiv:2204.02425`] [ɪɴSPIRE].

[36] C. Pallis, *E- and T-model hybrid inflation*, *Eur. Phys. J. C* **83** (2023) 2 [`arXiv:2209.09682`] [ɪɴSPIRE].

[37] C. Carbone and S. Matarrese, *A Unified treatment of cosmological perturbations from super-horizon to small scales*, *Phys. Rev. D* **71** (2005) 043508 [`astro-ph/0407611`] [ɪɴSPIRE].

[38] K.N. Ananda, C. Clarkson and D. Wands, *The Cosmological gravitational wave background from primordial density perturbations*, *Phys. Rev. D* **75** (2007) 123518 [`gr-qc/0612013`] [ɪɴSPIRE].

[39] D. Baumann, P.J. Steinhardt, K. Takahashi and K. Ichiki, *Gravitational Wave Spectrum Induced by Primordial Scalar Perturbations*, *Phys. Rev. D* **76** (2007) 084019 [`hep-th/0703290`] [ɪɴSPIRE].

[40] G. Domènech, *Scalar Induced Gravitational Waves Review*, *Universe* **7** (2021) 398 [`arXiv:2109.01398`] [ɪɴSPIRE].

[41] PLANCK collaboration, *Planck 2018 results. X. Constraints on inflation*, *Astron. Astrophys.* **641** (2020) A10 [`arXiv:1807.06211`] [ɪɴSPIRE].

[42] BICEP and KECK collaborations, *Improved Constraints on Primordial Gravitational Waves using Planck, WMAP, and BICEP/Keck Observations through the 2018 Observing Season*, *Phys. Rev. Lett.* **127** (2021) 151301 [`arXiv:2110.00483`] [ɪɴSPIRE].

[43] D. Paoletti, F. Finelli, J. Valiviita and M. Hazumi, *Planck and BICEP/Keck Array 2018 constraints on primordial gravitational waves and perspectives for future B-mode polarization measurements*, *Phys. Rev. D* **106** (2022) 083528 [`arXiv:2208.10482`] [ɪɴSPIRE].

[44] S. Clesse and J. García-Bellido, *Massive Primordial Black Holes from Hybrid Inflation as Dark Matter and the seeds of Galaxies*, *Phys. Rev. D* **92** (2015) 023524 [`arXiv:1501.07565`] [ɪɴSPIRE].

[45] PLANCK collaboration, *Planck 2013 results. XXII. Constraints on inflation*, *Astron. Astrophys.* **571** (2014) A22 [`arXiv:1303.5082`] [ɪɴSPIRE].

[46] LIGO SCIENTIFIC and VIRGO collaborations, *Observation of Gravitational Waves from a Binary Black Hole Merger*, *Phys. Rev. Lett.* **116** (2016) 061102 [`arXiv:1602.03837`] [ɪɴSPIRE].

[47] S. Bird et al., *Did LIGO detect dark matter?*, *Phys. Rev. Lett.* **116** (2016) 201301 [`arXiv:1603.00464`] [ɪɴSPIRE].

[48] M. Sasaki, T. Suyama, T. Tanaka and S. Yokoyama, *Primordial Black Hole Scenario for the Gravitational-Wave Event GW150914*, *Phys. Rev. Lett.* **117** (2016) 061101 [*Erratum ibid.* **121** (2018) 059901] [`arXiv:1603.08338`] [ɪɴSPIRE].

[49] S. Clesse and J. García-Bellido, *The clustering of massive Primordial Black Holes as Dark Matter: measuring their mass distribution with Advanced LIGO*, *Phys. Dark Univ.* **15** (2017) 142 [`arXiv:1603.05234`] [ɪɴSPIRE].

[50] R. Kallosh and A. Linde, *Universality Class in Conformal Inflation*, *JCAP* **07** (2013) 002 [`arXiv:1306.5220`] [ɪɴSPIRE].

[51] S. Ferrara, R. Kallosh, A. Linde and M. Porrati, *Minimal Supergravity Models of Inflation*, *Phys. Rev. D* **88** (2013) 085038 [`arXiv:1307.7696`] [ɪɴSPIRE].

[52] R. Kallosh, A. Linde and D. Roest, *Superconformal Inflationary α-Attractors*, *JHEP* **11** (2013) 198 [`arXiv:1311.0472`] [ɪɴSPIRE].

[53] R. Kallosh and A. Linde, *BICEP/Keck and cosmological attractors*, *JCAP* **12** (2021) 008 [`arXiv:2110.10902`] [ɪɴSPIRE].

[54] R. Kallosh and A. Linde, *Polynomial α-attractors*, *JCAP* **04** (2022) 017 [`arXiv:2202.06492`] [ɪɴSPIRE].

[55] D.K. Hazra, L. Sriramkumar and J. Martin, *BINGO: A code for the efficient computation of the scalar bi-spectrum*, *JCAP* **05** (2013) 026 [`arXiv:1201.0926`] [ɪɴSPIRE].

[56] M. Braglia, D.K. Hazra, L. Sriramkumar and F. Finelli, *Generating primordial features at large scales in two field models of inflation*, *JCAP* **08** (2020) 025 [`arXiv:2004.00672`] [ɪɴSPIRE].

[57] R. Kallosh and A. Linde, *Escher in the Sky*, *Comptes Rendus Physique* **16** (2015) 914 [`arXiv:1503.06785`] [ɪɴSPIRE].

[58] A.D. Linde, *Chaotic Inflation*, *Phys. Lett. B* **129** (1983) 177 [ɪɴSPIRE].

[59] A.D. Linde, *Initial conditions for inflation*, *Phys. Lett. B* **162** (1985) 281 [ɪɴSPIRE].

[60] A. Linde, *On the problem of initial conditions for inflation*, *Found. Phys.* **48** (2018) 1246 [`arXiv:1710.04278`] [ɪɴSPIRE].

[61] G.N. Felder, L. Kofman and A.D. Linde, *Inflation and preheating in NO models*, *Phys. Rev. D* **60** (1999) 103505 [`hep-ph/9903350`] [ɪɴSPIRE].

[62] S. Clesse and J. Rocher, *Avoiding the blue spectrum and the fine-tuning of initial conditions in hybrid inflation*, *Phys. Rev. D* **79** (2009) 103507 [`arXiv:0809.4355`] [ɪɴSPIRE].

[63] P.J. Steinhardt, *Natural Inflation*, in *Nuffield Workshop on the Very Early Universe*, 21 June – 9 July 1982, Cambridge, United Kingdom [ɪɴSPIRE]].

[64] A.D. Linde, *Nonsingular regenerating inflationary universe*, Print-82-0554, Cambridge (1982) [ɪɴSPIRE].

[65] A. Vilenkin, *The Birth of Inflationary Universes*, *Phys. Rev. D* **27** (1983) 2848 [ɪɴSPIRE].

[66] A.D. Linde, *Eternally Existing Selfreproducing Chaotic Inflationary Universe*, *Phys. Lett. B* **175** (1986) 395 [ɪɴSPIRE].

[67] A.D. Linde, *Monopoles as big as a universe*, *Phys. Lett. B* **327** (1994) 208 [`astro-ph/9402031`] [ɪɴSPIRE].

[68] A. Vilenkin, *Topological inflation*, *Phys. Rev. Lett.* **72** (1994) 3137 [`hep-th/9402085`] [ɪɴSPIRE].

[69] A.D. Linde and D.A. Linde, *Topological defects as seeds for eternal inflation*, *Phys. Rev. D* **50** (1994) 2456 [`hep-th/9402115`] [ɪɴSPIRE].

[70] N. Sakai, H.-A. Shinkai, T. Tachizawa and K.-I. Maeda, *Dynamics of topological defects and inflation*, *Phys. Rev. D* **53** (1996) 655 [*Erratum ibid.* **54** (1996) 2981] [`gr-qc/9506068`] [ɪɴSPIRE].

[71] A.D. Linde, *Fast roll inflation*, *JHEP* **11** (2001) 052 [`hep-th/0110195`] [ɪɴSPIRE].

[72] A.A. Starobinsky, *Stochastic de Sitter (inflationary) stage in the early universe*, *Lect. Notes Phys.* **246** (1986) 107 [ɪɴSPIRE].

[73] A.S. Goncharov, A.D. Linde and V.F. Mukhanov, *The Global Structure of the Inflationary Universe*, *Int. J. Mod. Phys. A* **2** (1987) 561 [ɪɴSPIRE].

[74] A.D. Linde, D.A. Linde and A. Mezhlumian, *From the Big Bang theory to the theory of a stationary universe*, *Phys. Rev. D* **49** (1994) 1783 [`gr-qc/9306035`] [ɪɴSPIRE].

[75] J. Garcia-Bellido, A.D. Linde and D.A. Linde, *Fluctuations of the gravitational constant in the inflationary Brans-Dicke cosmology*, *Phys. Rev. D* **50** (1994) 730 [`astro-ph/9312039`] [ɪɴSPIRE].

[76] G.N. Felder et al., *Dynamics of symmetry breaking and tachyonic preheating*, *Phys. Rev. Lett.* **87** (2001) 011601 [`hep-ph/0012142`] [InSPIRE].

[77] G.N. Felder, L. Kofman and A.D. Linde, *Tachyonic instability and dynamics of spontaneous symmetry breaking*, *Phys. Rev. D* **64** (2001) 123517 [`hep-th/0106179`] [InSPIRE].

[78] F. Finelli et al., *Generation of fluctuations during inflation: Comparison of stochastic and field-theoretic approaches*, *Phys. Rev. D* **79** (2009) 044007 [`arXiv:0808.1786`] [InSPIRE].

[79] F. Finelli et al., *Stochastic growth of quantum fluctuations during slow-roll inflation*, *Phys. Rev. D* **82** (2010) 064020 [`arXiv:1003.1327`] [InSPIRE].

[80] V. Demozzi, A. Linde and V. Mukhanov, *Supercurvaton*, *JCAP* **04** (2011) 013 [`arXiv:1012.0549`] [InSPIRE].

[81] M. Kawasaki and Y. Tada, *Can massive primordial black holes be produced in mild waterfall hybrid inflation?*, *JCAP* **08** (2016) 041 [`arXiv:1512.03515`] [InSPIRE].

[82] H. Assadullahi et al., *Multiple Fields in Stochastic Inflation*, *JCAP* **06** (2016) 043 [`arXiv:1604.04502`] [InSPIRE].

[83] L. Pinol, S. Renaux-Petel and Y. Tada, *A manifestly covariant theory of multifield stochastic inflation in phase space: solving the discretisation ambiguity in stochastic inflation*, *JCAP* **04** (2021) 048 [`arXiv:2008.07497`] [InSPIRE].

[84] M. Braglia et al., *Unified framework for early dark energy from α-attractors*, *Phys. Rev. D* **102** (2020) 083513 [`arXiv:2005.14053`] [InSPIRE].

[85] J.-Q. Jiang and Y.-S. Piao, *Toward early dark energy and ns=1 with Planck, ACT, and SPT observations*, *Phys. Rev. D* **105** (2022) 103514 [`arXiv:2202.13379`] [InSPIRE].

[86] J.S. Cruz, F. Niedermann and M.S. Sloth, *A grounded perspective on new early dark energy using ACT, SPT, and BICEP/Keck*, *JCAP* **02** (2023) 041 [`arXiv:2209.02708`] [InSPIRE].

[87] W. Giarè et al., *Is the Harrison-Zel'dovich spectrum coming back? ACT preference for $n_s \sim 1$ and its discordance with Planck*, `arXiv:2210.09018` [`DOI:10.1093/mnras/stad724`] [InSPIRE].

[88] M. Sasaki, T. Suyama, T. Tanaka and S. Yokoyama, *Primordial black holes — perspectives in gravitational wave astronomy*, *Class. Quant. Grav.* **35** (2018) 063001 [`arXiv:1801.05235`] [InSPIRE].

[89] A. Escrivà, F. Kuhnel and Y. Tada, *Primordial Black Holes*, `arXiv:2211.05767` [InSPIRE].

[90] A. Linde, S. Mooij and E. Pajer, *Gauge field production in supergravity inflation: Local non-Gaussianity and primordial black holes*, *Phys. Rev. D* **87** (2013) 103506 [`arXiv:1212.1693`] [InSPIRE].

[91] S. Wang, T. Terada and K. Kohri, *Prospective constraints on the primordial black hole abundance from the stochastic gravitational-wave backgrounds produced by coalescing events and curvature perturbations*, *Phys. Rev. D* **99** (2019) 103531 [*Erratum ibid.* **101** (2020) 069901] [`arXiv:1903.05924`] [InSPIRE].

[92] P.S. Cole, A.D. Gow, C.T. Byrnes and S.P. Patil, *Steepest growth re-examined: repercussions for primordial black hole formation*, `arXiv:2204.07573` [InSPIRE].

[93] D.J. Schwarz, C.A. Terrero-Escalante and A.A. Garcia, *Higher order corrections to primordial spectra from cosmological inflation*, *Phys. Lett. B* **517** (2001) 243 [`astro-ph/0106020`] [InSPIRE].

[94] C.T. Byrnes, P.S. Cole and S.P. Patil, *Steepest growth of the power spectrum and primordial black holes*, *JCAP* **06** (2019) 028 [`arXiv:1811.11158`] [InSPIRE].

[95] P. Carrilho, K.A. Malik and D.J. Mulryne, *Dissecting the growth of the power spectrum for primordial black holes*, *Phys. Rev. D* **100** (2019) 103529 [`arXiv:1907.05237`] [InSPIRE].

[96] M. Biagetti, M. Fasiello and A. Riotto, *Enhancing Inflationary Tensor Modes through Spectator Fields*, *Phys. Rev. D* **88** (2013) 103518 [`arXiv:1305.7241`] [InSPIRE].

[97] J. Fumagalli et al., *Primordial gravitational waves from excited states*, *JHEP* **03** (2022) 196 [`arXiv:2111.14664`] [InSPIRE].

[98] W. Zhao, Y. Zhang, X.-P. You and Z.-H. Zhu, *Constraints of relic gravitational waves by pulsar timing arrays: Forecasts for the FAST and SKA projects*, *Phys. Rev. D* **87** (2013) 124012 [`arXiv:1303.6718`] [InSPIRE].

[99] LISA Cosmology Working Group collaboration, *Cosmology with the Laser Interferometer Space Antenna*, `arXiv:2204.05434` [LISA CosWG-22-03] [InSPIRE].

[100] K. Yagi and N. Seto, *Detector configuration of DECIGO/BBO and identification of cosmological neutron-star binaries*, *Phys. Rev. D* **83** (2011) 044011 [*Erratum ibid.* **95** (2017) 109901] [`arXiv:1101.3940`] [InSPIRE].

[101] K. Kohri and T. Terada, *Semianalytic calculation of gravitational wave spectrum nonlinearly induced from primordial curvature perturbations*, *Phys. Rev. D* **97** (2018) 123532 [`arXiv:1804.08577`] [InSPIRE].

[102] J.R. Espinosa, D. Racco and A. Riotto, *A Cosmological Signature of the SM Higgs Instability: Gravitational Waves*, *JCAP* **09** (2018) 012 [`arXiv:1804.07732`] [InSPIRE].

[103] Planck collaboration, *Planck 2018 results. VI. Cosmological parameters*, *Astron. Astrophys.* **641** (2020) A6 [*Erratum ibid.* **652** (2021) C4] [`arXiv:1807.06209`] [InSPIRE].

[104] NANOGrav collaboration, *The NANOGrav 12.5 yr Data Set: Search for an Isotropic Stochastic Gravitational-wave Background*, *Astrophys. J. Lett.* **905** (2020) L34 [`arXiv:2009.04496`] [InSPIRE].

[105] Z.-C. Zhao and S. Wang, *Bayesian Implications for the Primordial Black Holes from NANOGrav's Pulsar-Timing Data Using the Scalar-Induced Gravitational Waves*, *Universe* **9** (2023) 157 [`arXiv:2211.09450`] [InSPIRE].

[106] C. Caprini et al., *Reconstructing the spectral shape of a stochastic gravitational wave background with LISA*, *JCAP* **11** (2019) 017 [`arXiv:1906.09244`] [InSPIRE].

[107] R. Flauger et al., *Improved reconstruction of a stochastic gravitational wave background with LISA*, *JCAP* **01** (2021) 059 [`arXiv:2009.11845`] [InSPIRE].

[108] S. Kachru et al., *Towards inflation in string theory*, *JCAP* **10** (2003) 013 [`hep-th/0308055`] [InSPIRE].

[109] R. Kallosh and A. Linde, *CMB targets after the latest Planck data release*, *Phys. Rev. D* **100** (2019) 123523 [`arXiv:1909.04687`] [InSPIRE].

[110] R. Kallosh, A. Linde and Y. Yamada, *Planck 2018 and Brane Inflation Revisited*, *JHEP* **01** (2019) 008 [`arXiv:1811.01023`] [InSPIRE].

[111] L. Randall, M. Soljacic and A.H. Guth, *Supernatural inflation: Inflation from supersymmetry with no (very) small parameters*, *Nucl. Phys. B* **472** (1996) 377 [`hep-ph/9512439`] [InSPIRE].

[112] M. Kawasaki, N. Sugiyama and T. Yanagida, *Primordial black hole formation in a double inflation model in supergravity*, *Phys. Rev. D* **57** (1998) 6050 [`hep-ph/9710259`] [InSPIRE].

[113] J. Yokoyama, *Chaotic new inflation and formation of primordial black holes*, *Phys. Rev. D* **58** (1998) 083510 [`astro-ph/9802357`] [InSPIRE].

[114] P.H. Frampton, M. Kawasaki, F. Takahashi and T.T. Yanagida, *Primordial Black Holes as All Dark Matter*, *JCAP* **04** (2010) 023 [`arXiv:1001.2308`] [InSPIRE].

[115] M. Kawasaki, A. Kusenko, Y. Tada and T.T. Yanagida, *Primordial black holes as dark matter in supergravity inflation models*, *Phys. Rev. D* **94** (2016) 083523 [`arXiv:1606.07631`] [InSPIRE].

[116] K.-Y. Choi, S.-B. Kang and R.N. Raveendran, *Reconstruction of potentials of hybrid inflation in the light of primordial black hole formation*, *JCAP* **06** (2021) 054 [`arXiv:2102.02461`] [InSPIRE].

[117] V.C. Spanos and I.D. Stamou, *Gravitational waves and primordial black holes from supersymmetric hybrid inflation*, *Phys. Rev. D* **104** (2021) 123537 [`arXiv:2108.05671`] [InSPIRE].

[118] S. Kawai and J. Kim, *Primordial black holes and gravitational waves from nonminimally coupled supergravity inflation*, *Phys. Rev. D* **107** (2023) 043523 [`arXiv:2209.15343`] [InSPIRE].

[119] A. Vilenkin, Y. Levin and A. Gruzinov, *Cosmic strings and primordial black holes*, *JCAP* **11** (2018) 008 [`arXiv:1808.00670`] [InSPIRE].

[120] T. Matsuda, *Primordial black holes from monopoles connected by strings*, *Astropart. Phys.* **30** (2009) 333 [`hep-ph/0509061`] [InSPIRE].

[121] J.J.M. Carrasco, R. Kallosh, A. Linde and D. Roest, *Hyperbolic geometry of cosmological attractors*, *Phys. Rev. D* **92** (2015) 041301 [`arXiv:1504.05557`] [InSPIRE].

[122] J.J.M. Carrasco, R. Kallosh and A. Linde, *α-Attractors: Planck, LHC and Dark Energy*, *JHEP* **10** (2015) 147 [`arXiv:1506.01708`] [InSPIRE].

[123] R. Kallosh, A. Linde, D. Roest and Y. Yamada, $\overline{D3}$ *induced geometric inflation*, *JHEP* **07** (2017) 057 [`arXiv:1705.09247`] [InSPIRE].

[124] R. Kallosh, A. Linde, T. Wrase and Y. Yamada, *IIB String Theory and Sequestered Inflation*, *Fortsch. Phys.* **69** (2021) 2100127 [`arXiv:2108.08492`] [InSPIRE].